AGU PUBLICATIONS

JGR

Journal of Geophysical Research: Space Physics

RESEARCH ARTICLE
10.1002/2015JA021437

Key Points:
- First multifluid MHD reconstruction of the termination shock
- The termination shock is a high-β low–Mach number dispersive shock wave
- Observational constraint on the pickup ion abundance and temperature

Correspondence to:
B. Zieger,
berci@bu.edu

Citation:
Zieger, B., M. Opher, G. Tóth, R. B. Decker, and J. D. Richardson (2015), Constraining the pickup ion abundance and temperature through the multifluid reconstruction of the Voyager 2 termination shock crossing, *J. Geophys. Res. Space Physics*, *120*, 7130–7153, doi:10.1002/2015JA021437.

Received 11 MAY 2015
Accepted 19 AUG 2015
Accepted article online 22 AUG 2015
Published online 26 SEP 2015

Constraining the pickup ion abundance and temperature through the multifluid reconstruction of the Voyager 2 termination shock crossing

Bertalan Zieger[1], Merav Opher[1,2], Gábor Tóth[3], Robert B. Decker[4], and John D. Richardson[5]

[1]Center for Space Physics, Boston University, Boston, Massachusetts, USA, [2]Astronomy Department, Boston University, Boston, Massachusetts, USA, [3]Department of Atmospheric, Oceanic, and Space Sciences, University of Michigan, Ann Arbor, Michigan, USA, [4]Applied Physics Laboratory, The Johns Hopkins University, Laurel, Maryland, USA, [5]Kavli Center for Astrophysics and Space Science, Massachusetts Institute of Technology, Cambridge, Massachusetts, USA

Abstract Voyager 2 observations revealed that the hot solar wind ions (the so-called pickup ions) play a dominant role in the thermodynamics of the termination shock and the heliosheath. The number density and temperature of this hot population, however, have remained unknown, since the plasma instrument on board Voyager 2 can only detect the colder thermal ion component. Here we show that due to the multifluid nature of the plasma, the fast magnetosonic mode splits into a low-frequency fast mode and a high-frequency fast mode. The coupling between the two fast modes results in a quasi-stationary nonlinear wave mode, the "oscilliton," which creates a large-amplitude trailing wave train downstream of the thermal ion shock. By fitting multifluid shock wave solutions to the shock structure observed by Voyager 2, we are able to constrain both the abundance and the temperature of the undetected pickup ions. In our three-fluid model, we take into account the nonnegligible partial pressure of suprathermal energetic electrons (0.022–1.5 MeV) observed by the Low-Energy Charged Particle Experiment instrument on board Voyager 2. The best fitting simulation suggests a pickup ion abundance of $20 \pm 3\%$, an upstream pickup ion temperature of 13.4 ± 2 MK, and a hot electron population with an apparent temperature of ~0.83 MK. We conclude that the actual shock transition is a subcritical dispersive shock wave with low Mach number and high plasma β.

1. Introduction

Voyager 1 and Voyager 2 are the first man-made objects to cross the termination shock in December 2004 and August/September 2007, respectively [*Stone et al.*, 2005, 2008]. At the time of the termination shock crossings, Voyager 2 had a working plasma instrument [*Richardson et al.*, 2008].

Before the Voyager observations, it was generally believed that the termination shock is the strongest shock in the solar system, a supercritical shock reflecting and accelerating pick up ions and anomalous cosmic ray particles. In situ measurements did not confirm this scenario. Voyager 2 observed a weak shock with a compression ratio of 1.7 [*Richardson et al.*, 2008; *Burlaga et al.*, 2008] and the predicted peak of anomalous cosmic rays at the termination shock was not observed [*Stone et al.*, 2008]. Moreover, the Voyager spacecraft did not observe radio waves from the termination shock, unlike in the case of the supercritical planetary bow shocks or the mostly supercritical interplanetary shocks. Observations suggest that the termination shock is more like a cosmic ray-mediated shock, where the flow speed starts to decrease well before the shock front due to the pressure gradient of energetic foreshock ions [*Florinski et al.*, 2009], which significantly weakens the actual shock transition. One could explain the preshock deceleration of the solar wind with a temporal variation as well, which cannot be ruled out on the basis of a single-spacecraft measurement, although such low speeds (~320 km/s) have not been seen by Voyager 2 since 1980.

Another puzzling result is that the solar wind flow remained superfast (faster than the fast magnetosonic speed) downstream of the termination shock contrary to the prediction of single-fluid magnetohydrodynamic (MHD) theory [*Richardson et al.*, 2008; *Li et al.*, 2008]. Based on the observed energy drop across the termination shock, it was suggested that roughly 80% of the solar wind flow energy is transferred to the hot pickup ion population [*Richardson et al.*, 2008].

Pickup ions can be created by charge exchange between solar wind ions and interstellar neutrals, which are subsequently swept along with or "picked up" by the magnetic field frozen in the solar wind flow. The other

two mechanisms of pickup ion production are electron impact ionization and photoionization, the latter being important only in the inner heliosphere. The ion distribution then consists of two components: a relatively cold "core" of solar origin, superimposed on a tenuous hot "halo" of interstellar pickup ions.

Three-fluid models of the solar wind predict that the thermal population cools adiabatically, while the hot population of interstellar pickup ions is maintained at high temperatures (of the order of 10^6 K) by the energy input of continued ionization and pickup [*Isenberg*, 1986; *Whang*, 1998; *Usmanov and Goldstein*, 2006]. Voyager 2 observations essentially measure the core temperature of the cold thermal population. The temperature of the pickup ions is therefore one of the unknowns that we constrain in this paper. The other unknown is the pickup ion abundance, i.e., the number of pickup ions divided by the total number of ions in a unit volume of the plasma, which is predicted to increase gradually with heliocentric distance and eventually surpass 50% in the heliosheath [*Isenberg*, 1986; *Whang*, 1998; *Usmanov and Goldstein*, 2006].

Here we show that the presence of the hot pickup ions will result in a distinct shock structure that strongly depends on their abundance and temperature. We identify such structure in Voyager 2 observations and constrain the abundance and temperature of the hot pickup ions on the basis of the high-resolution magnetic and thermal plasma measurements.

Most global models of the outer heliosphere treat the ion components of the solar wind as a single MHD fluid [*Opher et al*., 2006, 2009; *Pogorelov et al*., 2007; *Alouani-Bibi et al*., 2011; *Ratkiewicz and Grygorczuk*, 2008; *Izmodenov et al*., 2009]. These models do not yield a self-consistent description of the pickup ions; therefore, additional assumptions are needed to link the upstream pickup ion pressure with the downstream pickup ion pressure across the termination shock [*Zank et al*., 1996, 2010; *Fahr and Chalov*, 2008]. The truly self-consistent treatment of the thermodynamics of each ion species and electrons is implemented in multi-ion multifluid MHD models [*Harnett and Winglee*, 2006; *Glocer et al*., 2009; *Najib et al*., 2011; *Tóth et al*., 2012]. These models solve separate continuity, momentum, and energy equations for each ion species.

We adapted the multifluid Block-Adaptive-Tree Solar Wind Roe-Type Upwind Scheme (BATS-R-US) MHD code [*Tóth et al*., 2012] for local shock tube simulations of the termination shock, where thermal solar wind ions, pickup ions, and electrons are treated as separate fluids. This multifluid shock tube model is applied for the detailed reconstruction of the Voyager 2 termination shock crossing in order to pin down the unknown pickup ion parameters. We investigate two cases, the cold electron case and the hot electron case. In the first case, the partial pressure of suprathermal energetic electrons is neglected and the pressure of thermal electrons is assumed to be zero, which is known as the cold electron approximation. In the second case, the observed partial pressure of energetic electrons is included in the electron fluid, and a finite pressure is assumed for the total electron fluid.

The paper is organized as follows. The three-fluid MHD description of the solar wind plasma and its theoretical predictions are discussed in section 2, the numerical model of the termination shock and the method of constraining pickup ion parameters at the termination shock are explained in section 3, the results of fitting the multifluid simulations to the Voyager 2 observations are shown in section 4, and finally, our conclusions are presented in section 5.

2. Three-Fluid MHD Theory of the Solar Wind Plasma

In multifluid models of solar wind plasma, thermal solar wind ions, pickup ions, and electrons are treated as separate fluids. The fluid model assumes implicitly that the velocity distribution functions are isotropic and Maxwellian for both the thermal and the hot pickup ion components. Hybrid simulations, where electrons are described as a fluid and ions are treated as individual particles, have shown that the sum of the thermal solar wind and pickup ion distributions at the termination shock can be approximated with a 2-Maxwellian distribution [*Wu et al*., 2010]. Moreover, the Vasyliunas-Siscoe model of pickup ions [*Vasyliunas and Siscoe*, 1976] predicts that thermal ions and pickup ions are well separated in phase space in the outer heliosphere, which has been confirmed recently by New Horizons observations at 22 AU [*Randol et al*., 2013]. Although the broad pickup ion distribution overlaps the thermal proton distribution at very low energies, the bulk of the two distributions are well separated. The thermal proton distribution looks like a narrow beam in phase space as compared to the extended isotropic pickup ion distribution, so the number of pickup protons is negligible compared to the number of thermal protons around the peak of the thermal proton distribution [see *Randol*

et al., 2013, Figure 3]. Ion beams have been successfully described with multi-ion multifluid MHD models (see, e.g., *Sauer and Dubinin* [2003] or *Dubinin et al*. [2004]). Based on these results, describing the solar wind as multifluid plasma comprising cold thermal solar wind ions, hot pickup ions, and electrons is a reasonable approximation. Indeed, as we will show below, the multifluid model produces remarkable agreement with observations. Kinetic effects are absent in our model, but we do capture the fluid character of the interaction between the two ion components.

In *Giacalone and Decker* [2010], pickup proton injection and acceleration at the termination shock was simulated with a time-dependent 2-D hybrid code using as input the plasma and field conditions measured at the Voyager 2 termination shock crossing. In addition to thermal solar wind protons, incident proton populations included freshly ionized core pickup protons (25% of the total ion density) and a suprathermal power law tail with form v^{-5}, with its intensity set to background levels measured upstream of the shock crossing. All proton populations contribute to the self-consistent simulations and each was tracked separately throughout the simulation. Energy spectra accumulated over the region downstream of the termination shock at the end of the simulation run [*Giacalone and Decker*, 2010; *Giacalone et al*., 2012] showed that self-consistent acceleration of the pickup proton core population was sufficient to reproduce the lower energy Voyager 2 Low-Energy Charged Particle Experiment (LECP) data.

Recent kinetic simulations [*Ariad and Gedalin*, 2013] use Liouville mapping of pickup ion test particles in a stationary termination shock structure to find the downstream pickup ion distribution. They came to the conclusion that the contribution of the high-energy tail of pickup ions is negligible at the shock transition, although this population does contribute to decelerating the solar wind upstream of the shock [*Florinski et al*., 2009]. The pressure balance is principally determined by the low-energy body of pickup ions, which further justifies our multifluid approach. They showed that the upstream density of pickup ions should be comparable to the thermal solar wind density in order to ensure pressure balance. They found a lower limit of 0.4 for the density ratio of pickup ions and thermal ions.

We use the following set of multi-ion multifluid MHD equations [*Glocer et al*., 2009] to describe the three-fluid solar wind model with thermal ions (SW), pickup ions (PUI), and electrons:

$$\frac{\partial \rho_j}{\partial t} + \nabla\cdot\left(\rho_j \mathbf{u}_j\right) = 0, \tag{1}$$

$$\frac{\partial\left(\rho_j \mathbf{u}_j\right)}{\partial t} + \nabla\cdot\left(\rho_j \mathbf{u}_j \mathbf{u}_j + p_j \tilde{\mathbf{I}}\right) = n_j q_j \left(\mathbf{u}_j - \mathbf{u}_+\right)\times\mathbf{B} + \frac{n_j q_j}{n_e e}\left(\mathbf{J}\times\mathbf{B} - \nabla p_e\right), \tag{2}$$

$$\frac{\partial \varepsilon_j}{\partial t} + \nabla\cdot\left[\left(\varepsilon_j + p_j\right)\mathbf{u}_j\right] = \mathbf{u}_j\cdot\left[n_j q_j \left(\mathbf{u}_j - \mathbf{u}_+\right)\times\mathbf{B} + \frac{n_j q_j}{n_e e}\left(\mathbf{J}\times\mathbf{B} - \nabla p_e\right)\right], \tag{3}$$

$$\frac{\partial \mathbf{B}}{\partial t} + \nabla\times\left(-\mathbf{u}_+\times\mathbf{B}\right) = 0, \tag{4}$$

$$\frac{\partial p_e}{\partial t} + \nabla\cdot\left(p_e \mathbf{u}_e\right) = -\left(\gamma - 1\right) p_e \nabla\mathbf{u}_e. \tag{5}$$

where ρ, n, q, $\mathbf{u}$, and p are mass density, number density, electric charge, velocity, and thermal pressure, respectively; index j stands for the two ion fluids (SW and PUI), and subscript e stands for the electron fluid; $\mathbf{B}$ is the magnetic field vector; $\mathbf{J} = \nabla\times\mathbf{B}/\mu_0$ is the current density; μ_0 is the permeability of free space; e is the elementary charge; $\gamma = 5/3$ is the adiabatic index; ε_j is the energy density of ion fluid j, defined as

$$\varepsilon_j = \frac{\rho_j u_j^2}{2} + \frac{p_j}{\gamma - 1}; \tag{6}$$

and $\mathbf{u}_+$ is the charge averaged ion velocity, defined as

$$\mathbf{u}_+ = \frac{\sum_j n_j q_j \mathbf{u}_j}{\sum_j n_j q_j}. \tag{7}$$

We solve a similar set of equations in the hot electron case, where the massless electron fluid is a mixture of thermal electrons and suprathermal energetic electrons. In this case, n_e, p_e, and $\boldsymbol{u}_e$ are replaced with the

apparent electron density n_e^*, the apparent electron pressure p_e^*, and the apparent electron velocity $\boldsymbol{u}_e^*$, respectively, where

$$n_e^* = n_e + n_{ec} \approx n_e; \tag{8}$$

$$p_e^* = p_e + p_{ec}; \tag{9}$$

$$u_e^* = \frac{n_e e \mathbf{u}_e + n_{ec} e \mathbf{u}_{ec}}{n_e e + n_{ec} e} \approx \mathbf{u}_e \tag{10}$$

and n_{ec}, p_{ec}, and $\boldsymbol{u}_{ec}$ are the number density, partial pressure, and flow velocity of the suprathermal energetic electrons. Thus, the third fluid is equivalent to a massless electron fluid with an apparent electron pressure of p_e^*. The gyroradius of a relativistic 1.5 MeV electron with 90° pitch angle upstream of the termination shock ($B = 0.067$ nT) is 9.7×10^4 km, while the gyroradius of a 0.022 MeV electron is 7.5×10^3 km. These electron gyroradii are comparable to or less than the gyroradius of an upstream pickup proton (~4×10^4 km) and an order of magnitude smaller than the wavelength of the oscilliton. This justifies that the partial pressure of energetic electrons (0.022–1.5 MeV) observed by the LECP instrument on board Voyager 2 can be included in the shock adiabatic equation of the total fluid across the termination shock (see equation (18) in section 3.3).

Although energetic ions (0.028–3.5 MeV) observed by LECP have a significant partial pressure contribution to the total plasma pressure as shown by *Decker et al*. [2008], we did not include this pressure in the multifluid Rankine-Hugoniot jump conditions at the termination shock crossing because the diffusion length scale of these particles is an order of magnitude larger than the characteristic length scale of the actual shock transition. Energetic ions can mediate the termination shock on length scales comparable to their diffusion length scale, but do not affect the jump conditions at the subshock [*Florinski et al*., 2009]. We estimated the diffusion length scale of energetic ions in Appendix A, based on three independent methods.

The Hall term and the electron pressure gradient term are neglected in the induction equation (4). Note that the momentum and energy equations, (2) and (3) cannot be written in conservative form, because of the n_j/n_e factors on the right-hand sides of the equations. This is because there is momentum and energy exchange between the fluids that are coupled through the magnetic field. The total momentum is, of course, conserved as can be seen by adding up the momentum equations (2). Similarly, adding up the energy equations (3) and $1/(\gamma - 1)$ times the electron pressure equation (5), one can obtain an equation for the total energy density $\varepsilon = \sum_j \varepsilon_j + p_e/(\gamma - 1)$ that is in conservation form except for terms proportional to $\mathbf{J} \times \mathbf{B}$.

As long as the magnetic energy density is small, as in the case at the termination shock, the total energy is properly conserved. We indeed verify that the model conserves the total energy as demonstrated in Figures 5b and 7b.

Linearizing the continuity and momentum equations (1) and (2), we can derive the following general dispersion relation of perpendicular magnetosonic waves in warm multifluid plasma (For the sake of completeness, the detailed derivation is included in Appendix B.):

$$\left(\sum_j \frac{\omega_{pj}^2 \Omega_j}{\omega^2 - c_j^2 k^2 - \Omega_j^2}\right)^2 - \left(c^2 k^2 + \sum_j \frac{\omega_{pj}^2 \left(\omega^2 - c_j^2 k^2\right)}{\omega^2 - c_j^2 k^2 - \Omega_j^2}\right)\left(\sum_j \frac{\omega_{pj}^2}{\omega^2 - c_j^2 k^2 - \Omega_j^2}\right) = 0, \tag{11}$$

where ω and k are the wave frequency and wave number, respectively, ω_{pj}, Ω_j, and c_j are the plasma frequency, the gyrofrequency and the sound speed of particle species j (see definitions in Appendix B), and c is the speed of light. In case of three fluids, i.e., thermal solar wind ions, pickup ions, and electrons, equation (11) reduces to a second-order polynomial equation in ω^2 (see equations (B21)–(B25); also given by *Toida and Aota* [2013]), which can be solved analytically. There are two linear plane wave solutions: a low-frequency fast mode and a high-frequency fast mode (see equations (B26) and (B27)). Thus, the multifluid nature of the plasma creates two kinds of fast magnetosonic waves, a low-frequency mode that propagates mainly in the cold thermal population, and a high-frequency mode that propagates mainly in the hot pickup ion population. In the following, the low-frequency fast mode will be referred to as solar wind ion fast mode (F_{SW}), and the high-frequency fast mode will be referred to as pickup ion fast mode (F_{PUI}). The phase velocities ($V_{ph} = \frac{\omega}{k}$) of the two linear wave modes (F_{SW} and F_{PUI}) are plotted in Figure 1a for the upstream conditions at the termination shock ($u_{SW1} = 320.7$ km/s, $n_{SW1} = 0.001278$ cm^{-3}, $T_{SW1} = 4155$ K, $B_1 = 0.06703$ nT, $n_{PUI1} = 0.25 n_{SW1}$, $T_{PUI1} = 13.4$ MK, and $p_{e1}^* = 0.0173$ pPa). Electron scale (yellow region in Figure 1) is defined as spatial

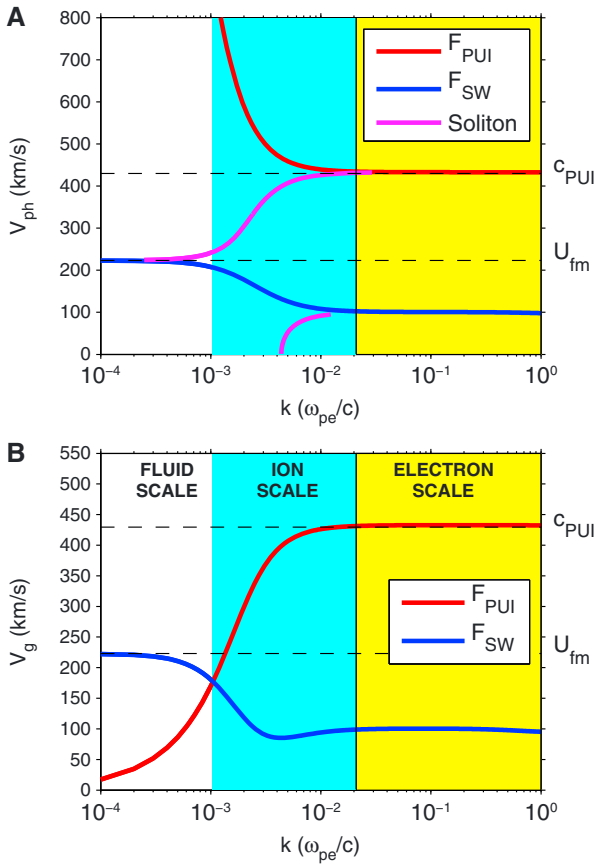

Figure 1. Fast magnetosonic wave modes propagating perpendicular to the magnetic field upstream of the termination shock, where the pickup ion abundance and temperature are 20% and 13.4 MK, respectively. (a) Phase velocities of the pickup ion fast mode F_{PUI}, the solar wind ion fast mode F_{SW}, and the quasi-stationary fast magnetosonic soliton mode. The soliton mode is coupled to F_{SW} at the fast magnetosonic speed of the total fluid (U_{fm}), resulting in a fast magnetosonic oscilliton mode on fluid scale. (b) Group velocities of F_{PUI} and F_{SW}. The critical speed of F_{SW} is U_{fm} at the low-frequency limit and the critical speed of F_{PUI} is c_{PUI} at the high-frequency limit, which predicts a double termination shocks in the three-fluid solar wind plasma if the solar wind flow is superfast in F_{PUI}, and a single termination shock if the solar wind is subfast in F_{PUI} and superfast in F_{SW}.

scales between the electron inertial length and the ion inertial length, where both thermal and pickup ions are demagnetized. Ion scale (cyan region in Figure 1) is defined as spatial scales of the order of the ion inertial length, where ion dynamics plays an important role in the velocity distributions. Fluid scale (white region in Figure 1) is defined as spatial scales where the velocity distribution of each ion and electron fluid can be approximated as a Maxwellian distribution. There is a gap in phase velocity, where linear waves cannot propagate. This is where quasi-stationary nonlinear wave solutions, solitons, and oscillitons exist [*Sauer et al.*, 2001, 2003; *Dubinin et al.*, 2006]. A soliton is a large-amplitude solitary structure that appears as a single peak or depression in the magnetic field and plasma parameters. An oscilliton, on the other hand, is a large-amplitude periodic structure that appears as a quasi-stationary wave train [*Sauer et al.*, 2001]. In order to get the phase velocity of quasi-stationary wave solutions, we need to solve the three-fluid plasma dispersion relation $D(\omega, k) = 0$ (equation (B21)) for k as a function of the phase velocity, $V_{ph} = \frac{\omega}{k}$. If the solution gives a real wave number, it is a linear plane wave. If the solution is imaginary, it is a soliton mode. Finally, if the solution gives a complex wave number, it is an oscilliton mode. Substituting the phase velocity in the dispersion relation, we obtain a third order polynomial equation for k^2 (equation (B28)) that can be solved analytically (see equations (B28)–(B-38)). The full set of wave number solutions (both real and imaginary parts) are plotted in Figure 2. The real solutions (blue and red lines in Figure 2) reproduce the low-frequency fast mode and the high-frequency fast mode plotted in Figure 1a. The phase velocity gap between the two is bridged by a fast magnetosonic soliton mode (magenta line in Figures 1a and 2). At the phase velocities where the soliton mode couples to the linear wave modes (F_{SW} and F_{PUI}, respectively), the wave number solution becomes complex, which produces an oscilliton mode. Thus, the three-fluid solar wind model predicts a fast magnetosonic oscilliton propagating at the fast magnetosonic speed of the total fluid (U_{fm}) and an ion acoustic oscilliton propagating at the sound speed of the pickup ion fluid (c_{PUI}).

The group velocities ($V_g = \frac{d\omega}{dk}$) of F_{PUI} and F_{SW} are plotted in Figure 1b, demonstrating the dispersive nature of both wave modes. There are two critical speeds: information cannot propagate faster than the fast magnetosonic speed of the total fluid ($U_{fm} = 223$ km/s) in the low-frequency fast mode (F_{SW}) and cannot propagate faster than the sound speed of the pickup ion fluid ($c_{PUI} = 430$ km/s) in the high-frequency fast mode (F_{PUI}). Thus, the three-fluid model of the solar wind predicts a double termination shock, one in the hot pickup ions and the other in the colder thermal ions, if the upstream flow velocity is greater than c_{PUI}. If the upstream flow velocity is less then c_{PUI} and greater than U_{fm}, there is only a single shock transition in the thermal ions. Both fast

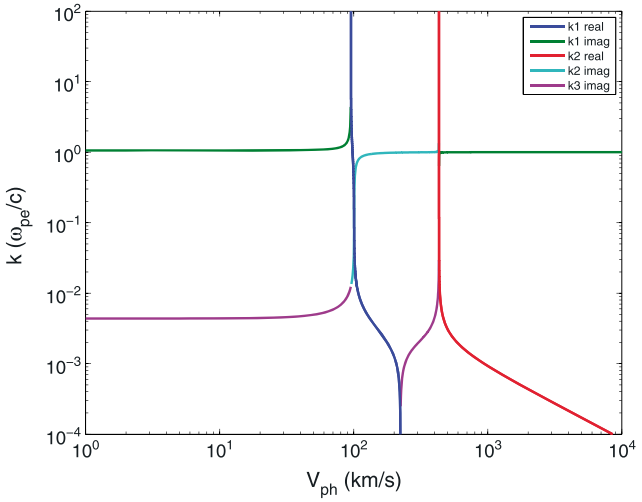

Figure 2. Wave number (k) solutions of the three-fluid (thermal ion, pickup ion, and electron) warm plasma dispersion relation for the same upstream conditions as in Figure 1. The real k solutions yield the low-frequency fast mode F_{SW} (k_1 real) and the high-frequency fast mode F_{PUI} (k_2 real), which are in fact ω_{SW}/V_{ph} and ω_{PUI}/V_{ph}, respectively. The imaginary k solutions yield the phase velocity of soliton modes, and the complex k solutions yield the phase velocity of oscilliton modes. Complex solutions exist at two phase velocities, where the fast magnetosonic soliton mode (k_3 imag) couples to the low-frequency and high-frequency fast modes (k_1 real and k_2 real), respectively.

modes are dispersive, which means that the group velocity V_g depends on the wave number k. F_{SW} is negative dispersive on fluid and ion scales, as its group velocity decreases with increasing k, while F_{PUI} is positive dispersive, as its group velocity increases with increasing k. Note that the superfast-subfast transition at the low-frequency limit occurs at the oscilliton velocity of U_{fm}, which was shown analytically as well in *Dubinin et al*. [2006].

An upstream propagating negative dispersive shock will produce a trailing wave train (quasi-stationary nonlinear wave or oscilliton) with a standing soliton (overshoot) at the shock front and a downstream propagating linear wave edge [*Hoefer*, 2014]. A positive dispersive shock, on the other hand, will produce a precursor wave train, with a linear wave edge in the upstream region and a standing soliton at the shock front. Such dispersive shock waves are solutions of the nonlinear Korteweg-de Vries equation of dispersive Eulerian fluids [*Biskamp*, 1973; *Hoefer*, 2014]. Since the fast magnetosonic oscilliton mode appears on fluid scale (see Figure 1a), our fluid model is able to capture the nonlinear trailing wave train of the thermal ion shock as we show below.

3. Methods

3.1. The Three-Fluid Shock Tube Model

We adapted the multifluid BATS-R-US MHD code [*Tóth et al*., 2012] for local shock tube simulations of the termination shock, where thermal solar wind ions, pickup ions, and electrons are treated as three separate fluids. Neutrals are not included in this model, because the charge exchange mean free path of neutrals (~50–100 AU) is much larger than the length scale of the termination shock. The governing multifluid MHD equations have been described in section 2. We solve separate continuity, momentum, and energy equations for each ion species and a separate equation for the electron pressure. This is a one-dimensional model, but we have three components for the vector quantities. The uniform grid contains 25,600 cells, and the cell size is 1000 km, less than the inertial length of thermal protons upstream of the termination shock (about 6300 km). We tested the grid convergence of the numerical model and obtained essentially the same numerical solution for 51,200 grid cells of 500 km in size. The initial left and right states of the shock tube are given by the upstream and downstream plasma parameters of the termination shock, where the downstream parameters are calculated from the Rankine-Hugoniot jump conditions for the total fluid (the mixture of cold thermal ions, hot pickup ions, and electrons). These boundary conditions result in a standing quasi-stationary shock solution in the simulation frame, which is in fact the shock frame. The two ion fluids are coupled by the magnetic field in the momentum and energy equations (see equations (2) and (3)), which can describe finite gyroradius effects [*Tóth et al*., 2012].

In the first set of simulations, we neglect the energetic electron pressure and use the cold electron approximation, assuming that the thermal speed of electrons is much less than the thermal speed of the ion species. The cold electron approximation is consistent with the Voyager 2 electron observations upstream of the termination shock that did not detect electrons in the energy range of the Plasma Science (PLS) instrument between 10 eV and 6 keV [*Richardson et al*., 2008].

Some recent theoretical works predict hot electrons in the solar wind at 100 AU [*Chashei and Fahr*, 2014; *Fahr et al*., 2014], but this prediction has not been confirmed by the in situ measurements. However, the LECP instrument on board Voyager 2 did detect a relatively high flux of energetic electrons in the three energy channels between 22 keV and 1.5 MeV [*Decker et al*., 2008], which could be the high-energy tail of a hot electron population at the termination shock. Most recently, *Fahr et al*. [2015] showed that a possible strong negative spacecraft potential might prevent the detection of medium-energy electrons by the Farady cups on board the Voyager spacecraft. In order to estimate the contribution of the energetic electrons to the thermodynamics of the termination shock crossing, we calculated the partial pressure of 0.022–1.5 MeV electrons from the corresponding differential intensities (see details in Appendix C). The partial pressure of energetic electrons (0.0033 pPa) turns out to be 2 orders of magnitude higher than the upstream thermal ion pressure (~10^{-5} pPa) and just 1 order of magnitude less than the upstream pickup ion pressure (~0.06 pPa). However, the number density of energetic electrons ($1.6\times10^{-7}\,\mathrm{cm}^{-3}$) is 4 orders of magnitude lower than the upstream thermal ion density ($1.3\times10^{-3}\,\mathrm{cm}^{-3}$). Since the differential intensity of energetic electrons is increasing toward lower energies [see *Decker et al*., 2008, Figure 1], we most probably underestimate the partial pressure of suprathermal electrons. In the second set of simulations, we include the apparent electron pressure (p_e^*) of suprathermal electrons in the electron fluid and refer to this case as the "hot electron case."

In each simulation, initially we ran a single-fluid multispecies model, where the flow velocity of thermal solar wind ions (u_{SW}) is forced to be the same as the flow velocity of pickup ions (u_{PUI}), which resulted in a standing single-fluid fast-mode shock in the shock tube frame. The multispecies solutions served as initial conditions for the multifluid simulations, and they also confirmed that the numerical model correctly reproduced the analytic jump conditions for the total fluid. Then we released the equal velocity constraint, allowing different velocities for thermal protons and pickup ions, and ran a truly multifluid simulation. The single-fluid fast-mode shock first split into a high-frequency fast-mode shock (or pickup ion shock) and a low-frequency fast-mode shock (or thermal ion shock) and after sufficiently long evolution we obtained quasi-stationary shock solutions in the shock frame. Depending on the upstream conditions, the quasi-stationary solution was either a double shock with shock transition (discontinuity) in both the pickup ions and the thermal ions or a single shock with shock transition only in the thermal ions. The thermal ion shock was always followed by a trailing wave train in the downstream region, as expected from the negative dispersive property of the low-frequency fast mode (F_{SW}).

The quasi-stationary structure of the termination shock is demonstrated in Figure 3a for different pairs of pickup ion number density (n_{PUI}) and temperature (T_{PUI}) satisfying the shock adiabatic equation of the total fluid (see equation (18) in section 3.3) in the cold electron case. Here the pickup ion number density is normalized to the thermal ion number density (n_{SW}) upstream of the termination shock. The magnetic field profiles consist of a "foot" starting at the marginal pickup ion shock, a "ramp," which is the actual thermal ion shock, an "overshoot," which is the standing soliton edge of the dispersive shock wave in the low-frequency fast-mode, and a "trailing wave train," which is a nonlinear quasi-stationary fast magnetosonic oscilliton propagating upstream at a group velocity that is the same as the downstream bulk flow velocity. The pickup ion shock appears as a small jump in the magnetic field, which is clearly seen at a distance of 10^5 km upstream of the thermal ion shock for the simulation with $n_{PUI}/n_{SW}=1$ (cyan line). Since the nonlinear oscilliton wave in the low-frequency fast mode F_{SW} has a maximum amplitude [*Toida and Aota*, 2013], the quasi-stationary waves can steepen into a discontinuity, also known as "shocklet," if the amplitude becomes larger than the maximum amplitude. Such nonlinear steepening, or sudden small jump in the magnetic field, is seen at the second peak of each trailing wave train plotted in Figure 3a. This is a time-dependent feature of the quasi-stationary shock solution. The amplitude of the trailing wave train oscillates in time around an average value and any wave peak can steepen temporarily into a shocklet. The magnitude of the overshoot, the amplitude of the oscilliton, and the wavelength of the oscilliton all depend on the pickup ion density. The average wavelength of the oscilliton is plotted in Figure 3c as a function of the pickup ion density. These properties of the oscilliton can be used to determine the unknown pickup ion parameters (density and temperature) from the actual termination shock crossings. The pickup ion density constrains the pickup ion temperature through the shock adiabatic equation, which can be obtained from the in situ Voyager 2 observations as explained in section 3.3.

3.2. Justifying the Perpendicular Shock Assumption

In our theoretical calculations and numerical simulations, we assumed that the termination shock is a perpendicular shock, i.e., the angle between the magnetic field and the shock normal (θ_{Bn}) is 90°. This assumption

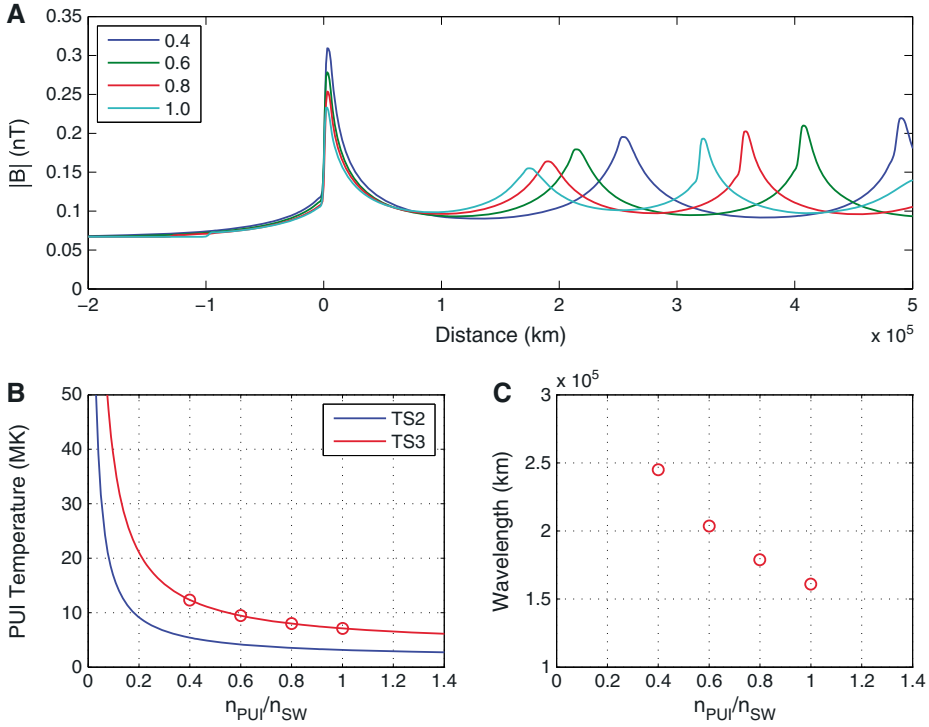

Figure 3. The effect of pickup ion density on the structure of the termination shock. (a) Simulated magnetic field profiles of the termination shock (TS3) for the normalized pickup ion number densities (n_{PUI}/n_{SW}) 0.4, 0.6, 0.8, and 1 in the cold electron case. The shock structure shows a foot, a ramp, an overshoot, and a nonlinear trailing wave train occasionally steepening into a shocklet. (b) Shock adiabatic curves in the pickup ion parameter space for the two termination shock crossings TS2 and TS3 in the cold electron case. All points [n_{PUI}, T_{PUI}] along each shock adiabatic curve would satisfy a shock with the observed compression ratio and shock speed. The shock wave solutions for four points along the shock adiabatic of TS3 (red circles) are plotted in Figure 3a. (c) Relationship between the wavelength of the oscilliton and the pickup ion number density derived from the numerical shock tube simulations.

needs to be verified by the Voyager 2 observations. Voyager 2 observed multiple termination shock crossings on 31 August and 1 September 2007 [*Richardson et al.*, 2008; *Li et al.*, 2008; *Burlaga et al.*, 2008]. The first crossing (TS1) occurred in a data gap, but there were high-resolution plasma and magnetic field observations during the second and third crossings (TS2 and TS3). In the following, we derive the shock normal ($\hat{\mathbf{n}}$) and θ_{Bn} both upstream and downstream of the termination shock crossing TS3 and calculate the uncertainty of $\hat{\mathbf{n}}$ and θ_{Bn} from the observed errors of the flow velocity ($\mathbf{u}$) and the magnetic field ($\mathbf{B}$). From single-spacecraft measurements, the shock normal can be obtained using the coplanarity theorem of the flow velocity [*Abraham-Shrauner*, 1972]:

$$\hat{\mathbf{n}} = \pm\frac{\mathbf{u}_2 - \mathbf{u}_1}{|\mathbf{u}_2 - \mathbf{u}_1|}, \tag{12}$$

the coplanarity theorem of the magnetic field [*Colburn and Sonett*, 1966]:

$$\hat{\mathbf{n}} = \pm\frac{(\mathbf{B}_2 - \mathbf{B}_1)\times(\mathbf{B}_2\times\mathbf{B}_1)}{|(\mathbf{B}_2 - \mathbf{B}_1)\times(\mathbf{B}_2\times\mathbf{B}_1)|}, \tag{13}$$

or the combination of these two [*Abraham-Shrauner*, 1972]:

$$\hat{\mathbf{n}} = \pm\frac{[\mathbf{B}_1\times(\mathbf{u}_2 - \mathbf{u}_1)]\times(\mathbf{B}_2 - \mathbf{B}_1)}{|[\mathbf{B}_1\times(\mathbf{u}_2 - \mathbf{u}_1)]\times(\mathbf{B}_2 - \mathbf{B}_1)|}, \tag{14}$$

where index 1 and index 2 refer to upstream and downstream parameters, respectively. We will refer to these methods as Methods 1–3, respectively. These methods assume that the upstream and downstream velocity and/or magnetic field vectors and the shock normal lie in the same plane. Method 1 is an approximation that is valid for high Alfven Mach number (M_A) shocks. Since the magnetic field intensity is very small at the

Table 1. Velocity and Magnetic Field Components Observed by Voyager 2 Upstream and Downstream of the Termination Shock Crossing TS3[a]

	Mean	Standard Deviation	Normalized Error
U_{R1}	320.7 km/s	1.8 km/s	0.6%
U_{T1}	12.5 km/s	3.9 km/s	1.2%
U_{N1}	−24.5 km/s	3.4 km/s	1.0%
U_{R2}	168.1 km/s	19.8 km/s	10.7%
U_{T2}	29.8 km/s	26.6 km/s	14.3%
U_{N2}	−51.3 km/s	45.9 km/s	24.8%
B_{R1}	−0.0116 nT	0.0045 nT	6.7%
B_{T1}	−0.0629 nT	0.0096 nT	14.4%
B_{N1}	−0.0181 nT	0.0069 nT	10.5%
B_{R2}	−0.0062 nT	0.0168 nT	13.6%
B_{T2}	−0.1225 nT	0.0276 nT	22.4%
B_{N2}	−0.0141 nT	0.0195 nT	15.8%

[a]Note that the normalized errors of the upstream velocity components are an order of magnitude smaller than the normalized errors of the upstream magnetic field components, which means that the direction of the velocity is much better defined than the direction of the magnetic field.

termination shock, M_A is expected to be high. Indeed, we found $M_A = 11.1$ for the total plasma fluid upstream of the shock and $M_A = 4.6$ downstream of the shock, which justifies the applicability of Method 1.

The observed upstream and downstream velocity and magnetic field components and their observed standard deviations (σ) are listed in Table 1. The normalized errors $\sigma/|\mathbf{u}|$ and $\sigma/|\mathbf{B}|$ are also listed in percentage so that the uncertainties in the velocity and magnetic field can be directly compared. The velocity and magnetic field components are given in RTN coordinates, which is a spacecraft centered coordinate system, where the unit vector $\hat{\mathbf{R}}$ points from the Sun to the spacecraft, $\hat{\mathbf{T}} = \hat{\Omega} \times \hat{\mathbf{R}}$, where $\hat{\Omega}$ is the unit vector in the direction of the solar rotation axis, and $\hat{\mathbf{N}}$ completes the right-handed set. The small normalized errors of the upstream velocity indicate that the direction of the velocity is well defined and less uncertain than the direction of the magnetic field. This implies that Method 1 must give a more accurate estimate of the shock normal than either Method 2 or Method 3. In addition, the observed upstream magnetic field intensity ($B = 0.067$ nT) is so weak that it is close to the sensitivity of the magnetometer. Since the uncertainty of each component of the magnetic field vector $\mathbf{B}$ is on the order of ±0.03 nT, the uncertainty in the magnetic field direction becomes large when B is on the order of 0.05 nT [*Burlaga and Ness*, 2009]. This means that the upstream magnetic field direction is poorly defined. The downstream magnetic field, on the other hand, can be regarded purely tangential within the measurement error (see Table 1).

Based on the above considerations, we used Method 1 to get the best estimate of the shock normal. We calculated the error of the shock normal from the observed 1σ errors of the upstream and downstream velocity components (listed in Table 1) using the error propagation formula:

$$\Delta\hat{\mathbf{n}} = \left|\frac{\partial\hat{\mathbf{n}}}{\partial u_{R1}}\Delta u_{R1}\right| + \left|\frac{\partial\hat{\mathbf{n}}}{\partial u_{T1}}\Delta u_{T1}\right| + \left|\frac{\partial\hat{\mathbf{n}}}{\partial u_{N1}}\Delta u_{N1}\right| + \left|\frac{\partial\hat{\mathbf{n}}}{\partial u_{R2}}\Delta u_{R2}\right| + \left|\frac{\partial\hat{\mathbf{n}}}{\partial u_{T2}}\Delta u_{T2}\right| + \left|\frac{\partial\hat{\mathbf{n}}}{\partial u_{N2}}\Delta u_{N2}\right|. \quad (15)$$

We obtained the shock normal $\hat{\mathbf{n}} = [0.9788 \pm 0.0802, -0.1109 \pm 0.2146, 0.1720 \pm 0.3333]$ in RTN coordinates. It is immediately seen that the shock normal is radial within the observation error. As a comparison, the global MHD model of the heliosphere by *Opher et al.* [2009] predicts $\hat{\mathbf{n}} = [0.9659, -0.2500, 0.0670]$ at the Voyager 2 termination shock crossing, which agrees with the observation within 1σ error.

Now we can calculate the angle between the upstream magnetic field and the shock normal as

$$\theta_{Bn1} = cos^{-1}\left(\frac{\mathbf{B}_1}{|\mathbf{B}_1|}\cdot\hat{\mathbf{n}}\right). \quad (16)$$

The error of θ_{Bn1} can be calculated from the observed errors of the upstream magnetic field components and the errors of the shock normal components through the error propagation formula:

$$\Delta\theta_{Bn1} = \left|\frac{\partial\theta_{Bn1}}{\partial B_{R1}}\Delta B_{R1}\right| + \left|\frac{\partial\theta_{Bn1}}{\partial B_{T1}}\Delta B_{T1}\right| + \left|\frac{\partial\theta_{Bn1}}{\partial B_{N1}}\Delta B_{N1}\right| + \left|\frac{\partial\theta_{Bn1}}{\partial n_R}\Delta n_R\right| + \left|\frac{\partial\theta_{Bn1}}{\partial n_T}\Delta n_T\right| + \left|\frac{\partial\theta_{Bn1}}{\partial n_N}\Delta n_N\right|. \quad (17)$$

The angle between the downstream magnetic field and the shock normal (θ_{Bn2}) and its error can be calculated in a similar way. This yields $\theta_{Bn1} = 83.5° \pm 17.6°$ and $\theta_{Bn2} = 87.6° \pm 18.1°$. So we can conclude that the termination shock crossing TS3 was indeed a perpendicular shock within the observation error. The magnetic field rotated away from the shock normal across the termination shock, which is a typical characteristic of fast magnetosonic shocks. Method 2 gives $\theta_{Bn1} = 65.1°$ and $\theta_{Bn2} = 76.9°$, while Method 3 gives $\theta_{Bn1} = 70.9°$ and $\theta_{Bn2} = 79.9°$, all of which fall within the error of Method 1. However, the authors do not trust Method 2 and 3 because of the large uncertainty of the upstream magnetic field direction. *Li et al*. [2008] used the Monte Carlo method to define the best fitting upstream and downstream conditions and found $\theta_{Bn1} = 88.3°$ and $\theta_{Bn2} = 88.9°$ for Method 1, which is very close to perpendicular. For Method 2 and Method 3, they obtained $\theta_{Bn1} = 70.0°$ and $\theta_{Bn2} = 77.4°$. However, no error estimates were given for these values. Based on the rigorous error analysis presented here, the authors are convinced that the termination shock crossing TS3 was very close to perpendicular, which justifies the perpendicular shock assumption used in this paper. Nevertheless, the dispersion relation of oblique fast magnetosonic waves in warm multifluid plasma can be easily derived in a similar way as described in Appendix B, which could be used in follow-up studies.

3.3. Constraining the Pickup Ion Parameters With the Shock Adiabatic Equation

The shock properties of the two termination shock crossings TS2 and TS3 were previously derived from the magnetic field and the plasma measurements assuming a single-fluid MHD model, where the conservation laws are assumed to be valid for the thermal component, yielding the Rankine-Hugoniot jump conditions for all MHD parameters. It was concluded that the termination shock is a low-β supercritical quasi-perpendicular shock ($\beta_{SW} = 0.04$ and $M_{fmSW} = 10$, where β_{SW} is the ratio of thermal and magnetic pressure and M_{fmSW} is the fast magnetosonic Mach number in the single thermal proton fluid), provided that the effect of pickup ions is negligible [*Li et al*., 2008; *Burlaga et al*., 2008]. Since the observed hydrodynamic energy of thermal ions is not conserved across the termination shock [*Li et al*., 2008], the Rankine-Hugoniot jump conditions, which are derived from the conservation laws, are not valid for the thermal ions. This fact casts serious doubt on the shock parameters derived from the single-fluid assumption and also challenges the interpretation of the termination shock as a low-β supercritical shock with high Mach number. Moreover, the solar wind flow remained superfast ($M_{fmSW} = 2.8$ for TS3) downstream of the shock [*Richardson et al*., 2008], which is not admissible in single-fluid MHD.

The conservation laws must be valid for the total fluid (the mixture of thermal ions, pickup ions, and electrons), therefore the Rankine-Hugoniot jump conditions must apply for the total fluid and not for the thermal ions, which allows momentum and energy transfer among the three-fluid components. In case of a perpendicular shock, the Rankine-Hugoniot jump conditions yield a compression ratio $q = \frac{\rho_2}{\rho_1} = \frac{B_2}{B_1} = \frac{u_1 - V_s}{u_2 - V_s}$, where ρ and u are the density and flow velocity of the total fluid, B is the magnetic field intensity, V_s is the shock speed, and the subscripts 1 and 2 refer to upstream and downstream values, respectively. The plasma parameters of the total fluid can be expressed in terms of the plasma parameters of the thermal ions and pickup ions as $\rho = \rho_{SW} + \rho_{PUI}$ and $p = p_{SW} + p_{PUI}$ for cold massless electrons. In the hot electron case, the total pressure includes the apparent electron pressure as well ($p = p_{SW} + p_{PUI} + p_e^*$). We can assume that pickup ions are fully picked up, i.e., there is no slippage between the average flow velocities in the perpendicular direction: $\langle u_{PUI} \rangle = \langle u_{SW} \rangle = \langle u_e \rangle = \langle u \rangle$, where $\langle\rangle$ represent fluid-scale averages over spatial scales much larger than the pickup ion gyroradius (about 4×10^4 km for a pickup ion temperature of 8.6 MK). From the continuity equations of the fluids we get $\frac{\langle \rho_2 \rangle}{\langle \rho_1 \rangle} = \frac{\langle \rho_{SW2} \rangle}{\langle \rho_{SW1} \rangle} = \frac{\langle \rho_{PUI2} \rangle}{\langle \rho_{PUI1} \rangle}$. So the compression ratio of the total fluid can be obtained from two independent Voyager 2 measurements, namely, $q = \frac{\langle \rho_{SW2} \rangle}{\langle \rho_{SW1} \rangle}$ and $q = \frac{\langle B_2 \rangle}{\langle B_1 \rangle}$. If q is known, we can get the shock speed V_s from the equation $q = \frac{\langle u_{SW1} \rangle - V_s}{\langle u_{SW2} \rangle - V_s}$, where $\langle u_{SW1} \rangle$ and $\langle u_{SW2} \rangle$ are the upstream and downstream bulk flow velocities measured by Voyager 2. We calculated the compression ratio for the termination shock crossings TS2 and TS3 (note that there was a data gap for TS1) from the Voyager 2 density and magnetic field measurements, yielding $q = 2.073$ for TS2 and $q = 1.784$ for TS3. The corresponding shock speeds are $V_s = 51.3$ km/s for TS2 and $V_s = -26.5$ km/s for TS3, which means that TS2 moved away from the Sun and TS3 moved toward the Sun. Since the upstream conditions apparently changed during the 4 h between the two crossings, we averaged the upstream conditions over only the 2 h directly following or preceding the corresponding shock crossing. For TS3 we obtained the upstream conditions $u_{SW1} = 320.7$ km/s,

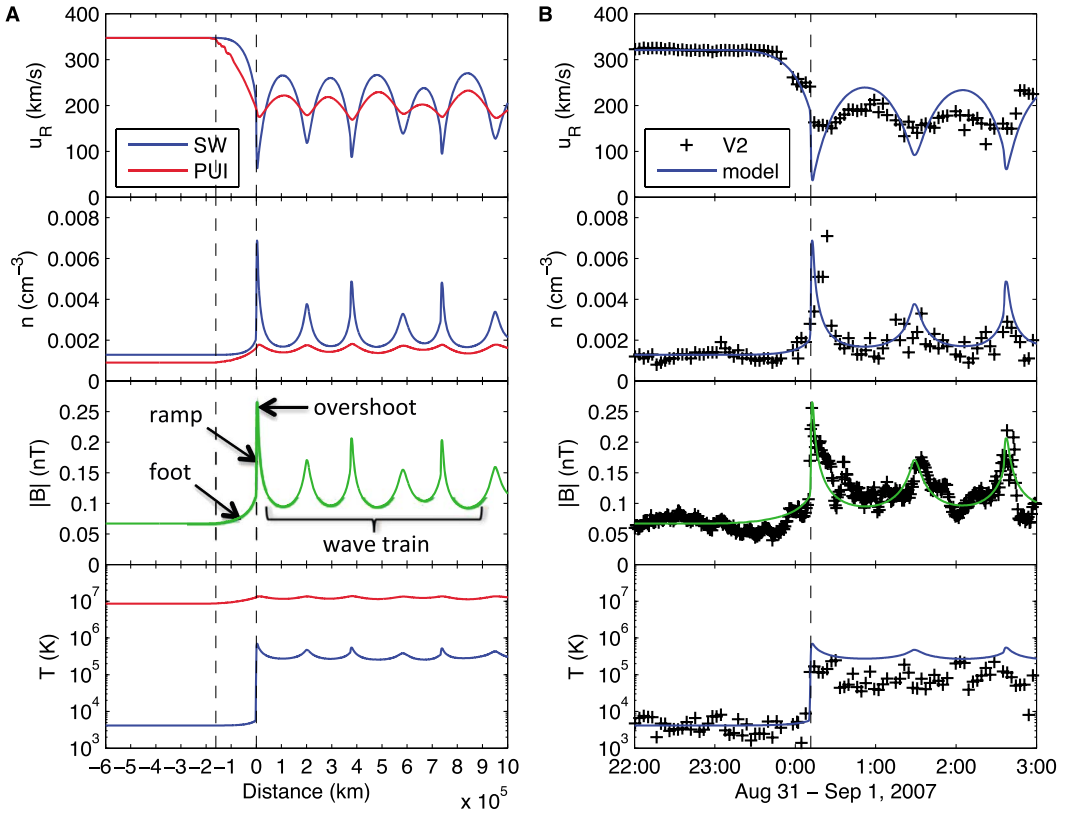

Figure 4. Multifluid structure of termination shock crossing TS3 in the cold electron case. (a) Quasi-stationary multifluid shock solution in the shock frame for a pickup ion abundance of 41% and the corresponding pickup ion temperature of 8.6 MK. The two vertical dashed lines mark the location of the marginal pickup ion shock and the thermal ion shock, respectively. The magnetic field profile consists of a foot, a ramp, an overshoot, and a quasi-stationary nonlinear "wave train." (b) Observed and simulated termination shock crossings of TS3. Black crosses (V2) are the Voyager 2 data and solid lines (model) are the corresponding parameters obtained from the quasi-stationary shock wave solution in Figure 4a.

$n_{SW1} = 0.001278\,\mathrm{cm}^{-3}$, $T_{SW1} = 4155\,\mathrm{K}$ and $B_1 = 0.0670\,\mathrm{nT}$. In case of TS2, the downstream conditions significantly changed during the 2 h before the shock crossing, which means that we cannot really assume a constant compression ratio and a constant shock speed for this crossing. Because of this temporal variation, we excluded TS2 from further analysis.

We can write the MHD shock adiabatic equation (see in text books, e.g., in *Fitzpatrick* [2014]) of the total fluid for a perpendicular shock as a function of the upstream sonic Mach number (M_1) and the upstream plasma β of the total fluid (β_1) as

$$2(2-\gamma)q^2 + \gamma\left[2(1+\beta_1) + (\gamma-1)\beta_1 M_1^2\right]q - \gamma(\gamma+1)\beta_1 M_1^2 = 0, \tag{18}$$

where $\beta_1 = \dfrac{2\mu_0\left(p_{SW1}+p_{PUI1}+p_{e1}^*\right)}{B_1^2}$ and $M_1 = \dfrac{(u_{SW1}-V_s)\sqrt{\rho_{SW1}+\rho_{PUI1}}}{\sqrt{\gamma\left(p_{SW1}+p_{PUI1}+p_{e1}^*\right)}}$.

Substituting $p_{PUI1} = n_{PUI1}k_B T_{PUI1}$ and $\rho_{PUI1} = m_p n_{PUI1}$ into equation (18), where k_B is the Boltzmann constant and m_p is the proton mass, we have only two unknowns, the upstream pickup ion number density (n_{PUI1}) and the upstream pickup ion temperature (T_{PUI1}). Now we can solve the shock adiabatic equation for the pickup ion temperature as a function of the pickup ion density. The solutions for TS2 and TS3 are plotted in Figure 3b in the case without energetic electron pressure ($p_{e1}^* = 0$). Here the pickup ion density is normalized to the upstream thermal ion density. All pairs of n_{PUI1} and T_{PUI1} along the shock adiabatic curve satisfy a shock in the total fluid with the given compression ratio and shock speed. Thus, we reduced the number of free parameters in our three-fluid model to one, namely, the pickup ion number density (n_{PUI1}). Similar curves can be obtained for the hot electron case with a nonzero apparent electron pressure p_{e1}^*. In the latter case, p_{e1}^* represents an additional free parameter in the model.

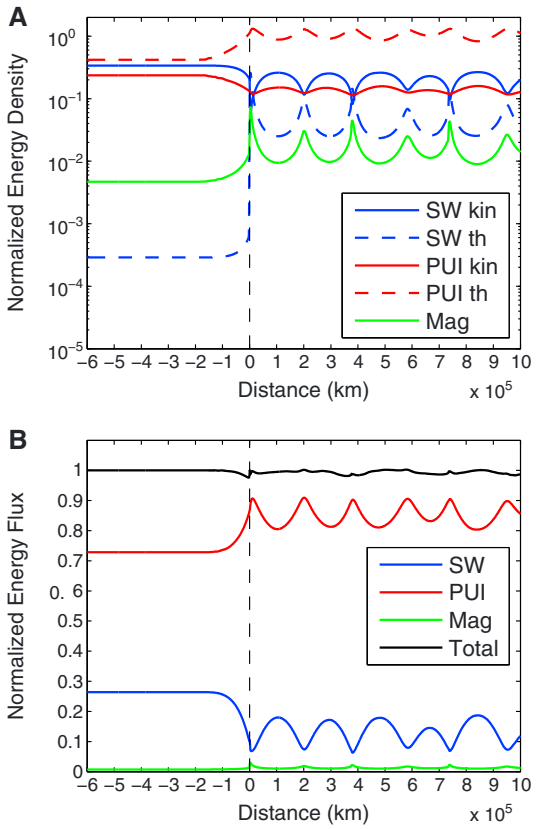

Figure 5. Energy partitioning across the termination shock (TS3) in the cold electron case. (a) Kinetic (kin) and thermal (th) energy densities of thermal solar wind ions (SW) and pickup ions (PUI), respectively, and the magnetic energy density (Mag) normalized to the total upstream energy density. Note that the upstream thermal energy density of PUI is higher than the kinetic energy density of SW. (b) Hydrodynamic energy fluxes of SW and PUI, respectively, and the magnetic energy flux (Mag) normalized to the total MHD energy flux (Total). The energy drop in SW is compensated by the energy gain in the PUI so that the total MHD energy is conserved.

4. Reconstruction of the Voyager 2 Termination Shock Crossing

We ran a series of simulations stepping in the pickup ion parameter space along the shock adiabatic curve of TS3 (see red curve in Figure 3b for the cold electron case) to obtain standing quasi-stationary shock wave solutions in the shock tube frame. Using the observed shock speed of TS3 ($V_s = -26.5$ km/s) and the radial speed of Voyager 2 (16.8 km/s), we calculated the relative velocity of Voyager 2 with respect to the shock front (43.3 km/s). Then we sampled our quasi-stationary shock solution in the shock frame by moving the spacecraft across the shock at this constant velocity to obtain a simulated time series for Voyager 2, which could be directly compared with the high-resolution magnetic and plasma observations. Here we assumed that the termination shock was quasi-stationary in the shock frame and the upstream conditions did not change significantly at least for 2 h after the crossing. We varied the pickup ion density and the corresponding pickup ion temperature until the wavelength of the trailing wave train matched the observed wavelength in the high-resolution magnetic data. In the cold electron case, the best fit between the simulated and observed termination shock crossings was obtained for 41% pickup ion abundance and 8.6 MK upstream pickup ion temperature (see Figure 4b). The multifluid model perfectly matches the length of the shock foot, the magnitude of the overshoot, the amplitude and wavelength of the oscilliton in the magnetic field, and even the nonlinear steepening of the second peak of the trailing wave train. There is a reasonable match between the observed and predicted thermal plasma parameters as well except that the cold electron model overestimates the amplitude of the oscilliton in the flow velocity as well as the heating of thermal ions across the termination shock. The full multifluid shock solution is presented in Figure 4a. Note that the thermal ion shock is not a discontinuity in the pickup ions and vice versa. The upstream Mach number for the low-frequency fast mode (F_{SW}) is 1.56, whereas the upstream Mach number for the high-frequency fast mode (F_{PUI}) is 1.01, indicating a marginal pickup ion shock. The temperature profiles demonstrate the preferential heating of thermal solar wind ions.

Unlike most of the single-fluid global models of the outer heliosphere, our local multifluid MHD model provides self-consistent energy partitioning among thermal ions pickup ions, and electrons across the termination shock. The hydrodynamic energy of each ion fluid component is not conserved in our model because of the coupling source terms on the right-hand side of the energy equation of each ion fluid (see equation (3)), which allow energy transfer between the two ion fluids. The energy partitioning for the best fitting multifluid shock solution of TS3 in the cold electron case is shown in Figure 5. The kinetic energy density is defined as $\frac{\rho u^2}{2}$, the thermal energy density is $\frac{p}{(\gamma-1)}$, the magnetic energy density is $\frac{B^2}{2\mu_0}$, and the total energy density (ε) is the sum of these three. The conserved quantity across the termination shock is the total MHD energy flux, defined here as $u\left(\varepsilon + p + \frac{B^2}{2\mu_0}\right)$, which is obtained from the conservative form of the MHD energy equation for a perpendicular shock.

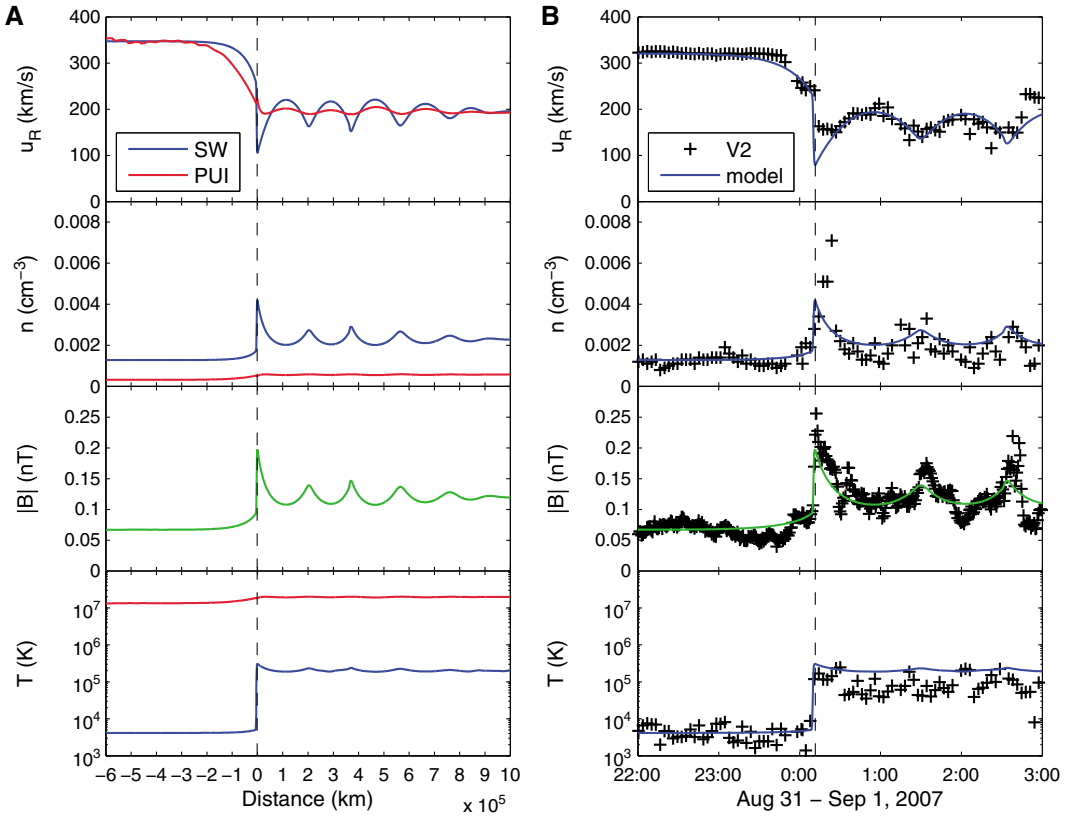

Figure 6. Multifluid structure of termination shock crossing TS3 in the hot electron case. (a) Quasi-stationary multifluid shock solution in the shock frame for a pickup ion abundance of 20%, a pickup ion temperature of 13.4 MK, and a suprathermal electron pressure of 0.0173 pPa. The vertical dashed lines mark the location of the thermal ion shock. There is no pickup ion shock in this case, because the upstream solar wind is subfast in the high-frequency fast mode due to the higher pickup ion temperature. (b) Observed and simulated termination shock crossings of TS3 in the same format as in Figure 4b.

In the cold electron case, the upstream thermal energy density of pickup ions is the highest with 42% of the total upstream energy density (Figure 5a). The kinetic energy density of thermal solar wind ions is only 34%, and the contribution of the kinetic energy density of pickup ions is as much as 24%. Thermal solar wind ions are preferentially heated across the termination shock as evidenced by the 2 orders of magnitude jump in their thermal energy density.

The hydrodynamic energy flux is not conserved across the termination shock for either of the ion components (see blue and red lines in Figure 5b). The decrease in the hydrodynamic energy flux of thermal solar wind ions is compensated by a comparable increase in the hydrodynamic energy flux of pickup ions to keep the total MHD energy flux conserved across the shock and within the trailing wave train (see black line in Figure 5b). In the cold electron case, 53% of the hydrodynamic energy flux of thermal solar wind ions is transferred to the heating of pickup ions. Voyager 2 observed a more substantial 77% drop in the hydrodynamic energy flux across the termination shock (TS3), which implies that the extra 24% energy drop is probably due to the heating of electrons or cold heavier ions (e.g., α particles).

In order to determine the effect of energetic electrons on the structure and thermodynamics of the termination shock, we included the partial pressure of energetic electrons in the massless electron fluid. We performed a two-parameter fitting to Voyager 2 observations by varying the upstream pickup ion number density (n_{PUI1}) and the apparent electron pressure (p^*_{e1}) to match both the wavelength and the amplitude of the nonlinear oscilliton wave observed in the radial component of the thermal ion velocity (u_R). The best fitting simulation in this so-called hot electron case is presented in Figure 6. The addition of a suprathermal electron pressure of 0.0173 pPa, corresponding to an apparent electron temperature of 0.83 MK, to the electron fluid resulted in a better fit to both the velocity and the temperature data (compare Figure 4b

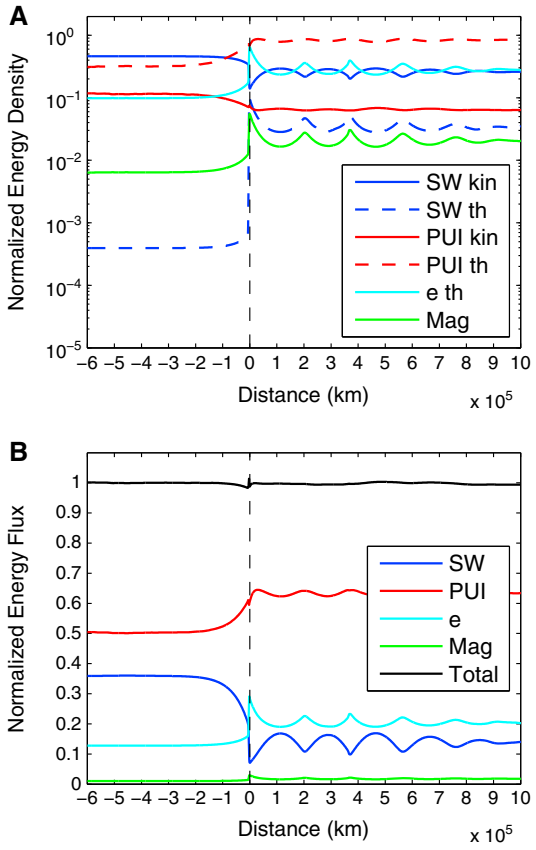

Figure 7. Energy partitioning across the termination shock (TS3) in the hot electron case. (a) Kinetic (kin) and thermal (th) energy densities of thermal solar wind ions (SW), pickup ions (PUI), and electrons (e), respectively, and the magnetic energy density (Mag) normalized to the total upstream energy density. Note that the downstream thermal energy density of electrons is comparable to the downstream kinetic energy density of SW. (b) Energy fluxes of SW, PUI, and electrons, respectively, and the magnetic energy flux (Mag) normalized to the total MHD energy flux (Total). The energy drop in SW is compensated by the energy gain in both the PUI and the electrons so that the total MHD energy is conserved.

and Figure 6b). The simulated downstream thermal ion temperature (2×10^5 K) is still somewhat higher than the temperature observed by Voyager 2 (10^5 K). A possible reason for this discrepancy could be that some of the upstream kinetic energy is transferred to the heating of α particles, which is not taken into account in our three-fluid MHD model. The pickup ion abundance reduced to $20 \pm 3\%$, and the upstream pickup ion temperature increased to 13.4 ± 2 MK. Since LECP observed only 0.0033 pPa energetic electron pressure, the extra pressure must come from a seed population of hot electrons at lower energies. These hot electrons may not be observed by the PLS instrument because of their low number density or because of a large negative spacecraft potential [*Fahr et al.*, 2015]. Our results support the conclusion of *Chalov and Fahr* [2013] concerning the significant role of shock-heated electrons in the pressure balance across the termination shock.

The self-consistent energy partitioning among the three fluids across the termination shock in the hot electron case is demonstrated in Figure 7. The upstream energy density is distributed among the kinetic energy density of thermal solar wind ions (46%), the thermal energy density of pickup ions (32%), the kinetic energy density of pickup ions (12%), and the energy density of electrons (10%) (see Figure 7a). The magnetic energy density and the thermal energy density of thermal ions are negligible. However, thermal ions are preferentially heated by 2 orders of magnitude across the termination shock. Surprisingly, pickup ions carry 50% of the total energy flux upstream of the termination shock, thermal solar wind ions only 36%, and the suprathermal electrons as much as 13% (see Figure 7b). The contribution of magnetic energy flux to the total MHD energy flux is only 1%, which is negligible. In the heliosheath, the pickup ion energy flux increases to 66%, the energy flux of electrons increases to 20% and the energy flux of thermal ions drops to as low as 12%. The kinetic energy of thermal solar wind ions goes not only to the heating of pickup ions but also to the heating of electrons. The total MHD energy is conserved across the termination shock (see black line in Figure 7). The 66% drop in the hydrodynamic energy of thermal ions is comparable to the 77% energy drop observed by Voyager 2. A part of the upstream kinetic energy may also transform into the preferential heating of minor cold ion populations (e.g., α particles), which are not included in our model.

5. Conclusions

The successful reconstruction of the termination shock crossing TS3 (see Figures 4b and 6b) indicates that the nonlinear trailing wave train observed on fluid scale by Voyager 2 is a quasi-stationary spatial structure in the reference frame of the termination shock. Based on the remarkable fit between our multifluid simulation and the Voyager 2 data, we can constrain the previously unknown pickup ion abundance and pickup ion temperature upstream of TS3. In the cold electron case, we obtained a relatively high pickup ion abundance of $41 \pm 3\%$ and a pickup ion temperature of 8.6 ± 0.7 MK. These results support the pressure balance

Table 2. Multifluid Shock Parameters of Termination Shock Crossing TS3 in the Cold Electron Case (Case 1) and the hot Electron Case (Case 2)[a]

	Case 1	Case 2
Compression ratio	1.784	1.784
Shock speed	−26.5 km/s	−26.5 km/s
Pickup ion abundance	41 ± 3%	20 ± 3%
Upstream pickup ion temperature	8.6 ± 0.7 MK	13.4 ± 2 MK
Downstream pickup ion temperature	12.6 ± 0.7 MK	20.4 ± 2 MK
Electron pressure	0.0000 pPa	0.0173 pPa
Critical speed of the low-frequency fast mode (U_{fm})	223 km/s	223 km/s
Critical speed of the high-frequency fast mode (c_{PUI})	344 km/s	430 km/s
Low-frequency fast Mach number	1.56	1.56
High-frequency fast Mach number	1.01	0.80
Upstream plasma β	59.5	43.4

[a]The termination shock is apparently a low-Mach number shock in high-β plasma. The plasma β is calculated for the total fluid including the partial pressures of thermal ions, pickup ions, and electrons.

considerations by *Ariad and Gedalin* [2013] showing that the pickup ion density should be comparable to the thermal ion density at the termination shock if the high-energy tail of the pickup ion distribution is neglected. The upstream pickup ion temperature of 8.6 ± 0.7 MK agrees with the prediction (~9 MK at 90 AU) of the latest three-fluid solar wind model [*Usmanov et al*., 2014] that includes eddy viscosity and turbulent resistivity but does not include the termination shock. In the hot electron case, we included the partial pressure of the observed LECP energetic electrons in the massless electron fluid and assumed a seed population of hot electrons at lower energies. The fit to the observed flow velocity and thermal ion temperature significantly improved with a suprathermal electron pressure of 0.0173 pPa (see Figure 6b), which corresponds to an apparent electron temperature of 0.83 MK. The best fit was obtained for a pickup ion abundance of 20 ± 3%, which is consistent with the theoretical prediction of charge exchange at the termination shock [*Fahr and Rucinski*, 1999]. The corresponding pickup ion temperature is 13.4 ± 2 MK, which is somewhat higher than predicted by recent solar wind models [e.g., *Usmanov et al*., 2014]. The higher pickup ion temperature could be due to particle acceleration processes in the preshock deceleration region of the energetic-particle-mediated termination shock. Or pickup ions could be heated across the predicted pickup ion shock upstream of the thermal ion shock. The upstream pickup ion thermal pressure from the best fitting simulation is 0.0592 pPa, which is 800 times higher than the observed upstream solar wind thermal pressure. As a comparison, *Randol et al*. [2013] predict a corresponding thermal pressure ratio of ~1000 at the termination shock on the basis of New Horizons pickup ion observations between 11 and 22 AU.

We conclude that the termination shock is not a single-fluid supercritical shock with high Mach number and low plasma β, as previously thought [*Richardson et al*., 2008; *Burlaga et al*., 2008], but a dispersive multifluid shock wave with low fast Mach number and high plasma β. The multifluid shock properties of TS3 are listed in Table 2 for the cold electron case (Case 1) as well as the hot electron case (Case 2). The upstream low-frequency fast Mach number of 1.56 indicates that the thermal ion shock is most certainly subcritical ($M_{fm} < 2.76$ for perpendicular shocks [see, e.g., *Balogh and Treumann,* 2013]). This means that most of the ions can cross the termination shock and ion reflection from the shock front is negligible. Therefore, temporal variations due to shock reformation observed at low-β supercritical quasi-perpendicular shocks are not expected at the termination shock. However, since the upstream hydrodynamic energy of the solar wind is dominated by the hydrodynamic energy of pickup ions (see Figure 7b) and the thermal energy of pickup ions dominates over the kinetic energy of pickup ions (see Figure 7a), the termination shock is very sensitive to temporal changes in the pickup ion temperature. Even if the solar wind flow is constant, the fast magnetosonic Mach number can change significantly due to changes in the pickup ion temperature. Generally, a shock moves away from the obstacle if the Mach number decreases, and moves toward the obstacle if the Mach number increases. This can be the reason for the temporal variability in the termination shock position, which can easily explain the observed multiple termination shock crossings.

The 1.01 value of the high-frequency fast Mach number indicates a marginal pickup ion shock in the cold electron case (Case 1). However, in the hot electron case (Case 2), the upstream solar wind is subfast in the high-frequency fast mode (F_{PUI}) and superfast in the low-frequency fast mode (F_{SW}), which means that TS3

is a single shock transition in the thermal ion component. Voyager 2 might have crossed a pickup ion shock further upstream of the thermal ion shock. This scenario is supported by Voyager 2 observations of several sudden drops in the hydrodynamic energy of the thermal solar wind component well before the actual termination shock crossing [see *Richardson et al*., 2008, Figure 4]. The reconstruction of these events is outside the scope of this study.

Our theoretical results are generally applicable for the thermodynamics of shocks in plasma environments where pickup ions are a major contributor, e.g., cometary bow shocks, bow shocks of unmagnetized planets, like Mars [*Sauer et al*., 1996; *Lu et al*., 2013], or other astrophysical shocks [*Soker et al*., 2010].

Appendix A: Estimating the Diffusion Length Scale of Energetic Ions at the Termination Shock

We use three different methods to estimate the diffusion length scale of energetic ions (0.028–3.5 MeV) observed by the LECP instrument on board Voyager 2 in order to determine whether the partial pressure of energetic ions should be included in the shock adiabatic equation of the termination shock: (1) we use the cosmic ray diffusion model by *Zank et al*. [1998] to obtain the theoretical prediction of the radial diffusion length scale λ_{rr} of energetic protons at 84 AU; (2) we extrapolate the empirical function of λ_{rr} for anomalous cosmic rays derived from Pioneer 10, Voyager 1, and Voyager 2 observations [*Fujii and McDonald*, 2005] to the lower rigidities of energetic ions; and (3) we calculate λ_{rr} for energetic ions from in situ Voyager 2 differential intensity measurements at the termination shock based on the method by *Florinski et al*. [2009].

Cosmic rays and energetic particles are tenuous compared to the background plasma; therefore, their mass and momentum densities can be neglected. Their transport in the heliosphere is usually described as the diffusion of a massless fluid in the solar wind plasma. The cosmic ray diffusion tensor consists of a parallel, a perpendicular, and a drift component [see, e.g., *Jokipii*, 1966]:

$$\widetilde{\kappa} = \begin{bmatrix} \kappa_{\perp} & \kappa_A & 0 \\ -\kappa_A & \kappa_{\perp} & 0 \\ 0 & 0 & \kappa_{||} \end{bmatrix}, \tag{A1}$$

where $\kappa_{||}$ and $\kappa_{\perp}$ describes diffusion along and perpendicular to the ambient magnetic field, respectively, while the off-diagonal antisymmetric element κ_A describes gradient and curvature drifts in the large-scale magnetic field. The radial diffusion coefficient in the heliosphere can be calculated as

$$\kappa_{rr} = \kappa_{||} cos^2\psi + \kappa_{\perp} sin^2\psi, \tag{A2}$$

where ψ is the winding angle of the Parker spiral heliospheric magnetic field [*Parker*, 1958]. The relevant quantity for the Voyager 2 termination shock crossing is the radial diffusion length scale λ_{rr} that describes the spatial scale of the interaction between the energetic particles and the background solar wind plasma. If λ_{rr} is much larger than the wavelength of the oscilliton, the partial pressure of energetic ions can be neglected in the shock adiabatic equation of the subshock (discontinuity in the background plasma), but it cannot be neglected on larger scale, i.e., in the foreshock region of the energetic-particle-mediated shock, where it contributes to the gradual deceleration of the solar wind flow [*Florinski et al*., 2009]. λ_{rr} is related to the radial diffusion coefficient at a given energy as follows:

$$\lambda_{rr} = 3\kappa_{rr}/v_c, \tag{A3}$$

where v_c is the equivalent speed of a relativistic cosmic ray particle (or energetic ion) of a given kinetic energy. *Zank et al*. [1998] evaluated the parallel, perpendicular, and drift components of the diffusion length scale, $\lambda_{||}$, $\lambda_{\perp}$, and λ_A, respectively, for different solar wind turbulence models as a function of rigidity (R) and radial distance from the Sun (r) [see *Zank et al*., 1998, equations (4)–(6)]. Rigidity is defined as the momentum (p) per unit charge (e) of the particle, and usually measured in MV or GV:

$$R = cp/Ze, \tag{A4}$$

where Z is the charge state and c is the speed of light. The particle rigidity is related to the particle rest energy E_0, and its kinetic energy E_k through the expression

$$R = \sqrt{E_k^2 + 2E_kE_0}. \tag{A5}$$

This parameter is very convenient to analyze particle movement in the magnetic field due to simple relations among particle rigidity, cyclotron frequency, and gyroradius. Different particles with the same rigidity follow identical paths in a given magnetic field. (In the following, we will make use of this property to estimate λ_{rr} for protons from the observed λ_{rr} of anomalous He^+ with the same rigidity.) *Zank et al.* [1998] concluded that λ_{rr} is dominated by $\lambda_{||}$ throughout the heliosphere, except for the pickup ion driven turbulence, where $\lambda_{\perp}$ becomes comparable to $\lambda_{||}$ in the outer heliosphere. In this model, $\lambda_{||} \propto R^{1/3}$ in the inner heliosphere, and $\lambda_{||} \propto R^2$ in the outer heliosphere, while $\lambda_{\perp} \propto R^2$ at all radial distances. Consequently, $\lambda_{rr} \propto R^2$ at the termination shock, which is due to the rigidity dependence of $\lambda_{||}$. Using this scaling relation, we can estimate the λ_{rr} of 0.028–3.5 MeV protons at the termination shock from the λ_{rr} of 100 MeV protons plotted in Figure 1 of [*Zank et al.*, 1998] for the case of nondriven turbulence:

$$\lambda_{rr} = \frac{\lambda_{rr0}}{R_0^2} R^2, \tag{A6}$$

where the reference values of the rigidity and the radial diffusion length scale at 84 AU are $R_0 = 445$ MV and $\lambda_{rr0} \approx 2.5$ AU. Equations (A5) and (A6) yields $\lambda_{rr} = 9.9 \times 10^4$ km for 0.028 MeV protons, $\lambda_{rr} = 1.2 \times 10^7$ km for 3.5 MeV protons, and $\lambda_{rr} = 1.1 \times 10^6$ km for the geometric mean energy of 0.313 MeV. Thus, cosmic ray diffusion theory predicts a radial diffusion length scale of the order of 10^6 km for the energetic ions observed by LECP. This distance is an order of magnitude larger than the spatial scale of the oscilliton wave (~10^5 km) and 2 orders of magnitude larger than the pickup ion gyroradius (~10^4 km).

Another way to determine λ_{rr} for energetic protons at the termination shock is to use anomalous cosmic ray measurements at different energies and different radial distances in the heliosphere to derive an empirical $\lambda_{rr}(r, R)$ function and extrapolate these results to the lower rigidity of energetic protons. For this purpose we can use anomalous cosmic ray particles different from protons, since λ_{rr} is the same for different particle species with the same rigidity, as mentioned above. *Fujii and McDonald* [2005] analyzed anomalous He^+ observations from Pioneer 10, Voyager1, and Voyager 2 at radial distances of 15.1 AU, 55 AU and 72 AU during the minima of solar cycles 20 and 22 in the rigidity range from 0.5 to 3 GV. They estimated the radial gradient of differential intensities (g_r) from the measurements of the three spacecraft and used the following formula to calculate λ_{rr} in three different energy channels (8.1 MeV/nucleon He^+, 15 MeV/nucleon He^+, and 42 MeV/nucleon He^+):

$$\lambda_{rr} = 3C v_{sw} / v_c g_r, \tag{A7}$$

where C is the Compton-Getting factor given by

$$C = -\frac{1}{3} \frac{\partial \ln f}{\partial \ln R} \tag{A8}$$

with $f = J/R^2$ and v_{sw} being the solar wind speed [*Cummings and Stone*, 2001]. Then they fitted a $\lambda_{rr} \propto R^{\alpha_1} r^{\alpha_2}$ scaling function to the observations, where α_1 and α_2 are the scaling exponents of the rigidity and the radial distance, respectively, and obtained the following empirical formula:

$$\lambda_{rr} = (1.4 \pm 0.9) \cdot 10^{-2} R^{1.6 \pm 0.1} r^{1.4 \pm 0.2}. \tag{A9}$$

Inserting the rigidity of 0.028–3.5 MeV protons (7.25–81.1 MV) and the radial distance of 84 AU to equation (A9), we get $\lambda_{rr} = 3.9 \times 10^5$ km for 0.028 MeV protons, $\lambda_{rr} = 1.9 \times 10^7$ km for 3.5 MeV protons, and $\lambda_{rr} = 2.7 \times 10^6$ km for 0.313 MeV protons. Note that this distance is comparable to the λ_{rr} predicted by the cosmic ray diffusion model of *Zank et al.* [1998]. Thus, the extrapolation of anomalous cosmic ray diffusion length scales to lower rigidities is consistent with the theoretical prediction.

Finally, we estimate λ_{rr} for energetic protons at the termination shock from in situ Voyager 2 measurements of 0.028–3.5 MeV protons. *Florinski et al.* [2009] determined κ_{rr} from the observed differential intensities in the energy channels 0.99–2.14 MeV and 2.14–3.50 MeV, assuming a steady state termination shock that is not moving in the inertial frame of reference, so that the time series of Voyager 2 can be readily converted into radial intensity profiles. They fitted a linear function to the logarithm of the observed differential intensity: $\log J(t) = a + bt$ with the parameters a and b, where t is the time, and calculated the radial diffusion coefficient from the following equation assuming a steady state diffusion solution and a constant solar wind speed of 350 km/s:

$$\kappa_{rr} = \frac{V_{sc} v_{sw}}{b \ln(10)}, \tag{A10}$$

where V_{sc} is the radial speed of the Voyager 2 spacecraft. They obtained $\kappa_{rr} = 10^{20}$ cm^2/s for energetic protons between 1 MeV and 3.5 MeV. Inserting this value into the definition of λ_{rr} (equation (A3)) we arrive at a third estimate of λ_{rr} for energetic protons at the termination shock, namely, $\lambda_{rr} = 1.6 \times 10^6$ km, which is in close agreement with the other two estimates. We acknowledge that all three methods have weaknesses due to the assumptions inherent in the given method. However, it is remarkable that they give approximately the same result. This strongly suggests that the diffusion length scale of 0.028–3.5 MeV energetic protons at the termination shock must be of the order of 10^6 km, which is 1 order of magnitude larger than the length scale of the nonlinear oscilliton wave and 2 orders of magnitude larger than the gyroradius of pickup ions. Thus, we justified that the partial pressure of energetic ions can be excluded from the generalized Rankine-Hugoniot jump conditions at the shock ramp of the thermal ion shock, which is, by the way, one of the underlying assumptions in the energetic-particle-mediated termination shock model by *Florinski et al.* [2009]. Nevertheless, the diffusion of energetic ions remains important on spatial scales much larger than 10^6 km and cannot be excluded from large-scale termination shock models that include the preshock deceleration region.

Appendix B: Derivation of the Phase Velocity of Solitons and Oscillitons

In the following we will derive the solution of the linear wave dispersion relation for a plasma consisting of thermal ions, pickup ions and electrons, using the upstream plasma parameters at the Voyager 2 termination shock crossing (TS3). The aim is to show that the trailing wave train observed by Voyager 2 downstream of the termination shock is a quasi-stationary wave structure, also known as oscilliton. This derivation is to obtain the wave number $\mathbf{k}$ as a function of the phase velocity V_{ph} in order to determine the phase velocity of quasi-stationary modes, solitons, and oscillitons. Note that this will give only the initial linear state of the soliton or oscilliton. The nonlinear growth rate and the full analytical solution of the oscilliton can be obtained from the nonlinear Korteweg-de Vries equation of dispersive Eulerian fluids [*Biskamp*, 1973; *Hoefer*, 2014]. The growth rate of the nonlinear low-frequency fast mode in a three-fluid model has been derived analytically by *Toida and Aota* [2013], and it has been shown that the low-frequency fast mode has a maximum amplitude. For the sake of completeness we also derive the general multifluid dispersion relation for perpendicular waves from the linearized continuity and momentum equations, which was not included in [*Toida and Aota*, 2013]. We start from the general dispersion relation, see, e.g., in *Baumjohann and Treumann* [1996],

$$\mathrm{Det}\left[\frac{k^2c^2}{\omega^2}\left(\frac{\mathbf{kk}}{k^2} - \widetilde{\mathbf{I}}\right) + \widetilde{\mathbf{M}}(\omega, \mathbf{k})\right] = 0, \tag{B1}$$

where $\widetilde{\mathbf{M}}$ is the dielectric tensor, which depends on the given plasma model, $\widetilde{\mathbf{I}}$ is the unit tensor, and c is the speed of light. We can choose a coordinate system where the ambient magnetic field is along the z axis, $\mathbf{B}_0 = B_0\hat{\mathbf{z}}$, and $k_y = 0$. In this case

$$\mathbf{k} = \begin{pmatrix} k_\perp \\ 0 \\ k_{||} \end{pmatrix} \text{ and } \mathbf{kk} = \begin{pmatrix} k_\perp^2 & 0 & k_{||}k_\perp \\ 0 & 0 & 0 \\ k_{||}k_\perp & 0 & k_{||}^2 \end{pmatrix}. \tag{B2}$$

For perpendicular wave propagation, $k_{||} = 0$, and the dispersion relation reduces to

$$\mathrm{Det}\left[\frac{k^2c^2}{\omega^2}\begin{pmatrix} 0 & 0 & 0 \\ 0 & -1 & 0 \\ 0 & 0 & -1 \end{pmatrix} + \widetilde{\mathbf{M}}(\omega, \mathbf{k})\right] = 0. \tag{B3}$$

We derive the dielectric tensor $\widetilde{\mathbf{M}}$ from the linearized continuity and momentum equations of thermal solar wind protons (SW), pickup ions (PUI), and electrons (e):

$$\frac{\partial n_j}{\partial t} + \nabla(n_j\mathbf{v}_j) = 0, \tag{B4}$$

$$m_j n_j \frac{\partial \mathbf{v}_j}{\partial t} = q_j n_j(\mathbf{E} + \mathbf{v}\times\mathbf{B}_0) - \nabla p_j, \tag{B5}$$

where m, n, $\mathbf{v}$, q, and p are mass, number density, velocity, charge, and thermal pressure of particle species j, which stands for the subscripts SW, PUI, and e. $\mathbf{E}$ is the electric field and $\mathbf{B}_0$ is the unperturbed magnetic field

along the z axis. Assuming plane wave-type linear perturbation $A_1(\mathbf{x}, t) = A_1(\mathbf{k}, \omega)\exp[i(\mathbf{kx} - \omega t)]$ propagating in the x direction, we get the linearized continuity equation

$$-i\omega n_{1j} + in_{0j}kv_{1xj} = 0, \tag{B6}$$

where index 1 and 0 denotes perturbed and unperturbed variables. Here we assumed that there is no slippage in bulk velocity between the particle species, i.e., $\mathbf{v}_{0j} = 0$ in the plasma frame. For perpendicular wave propagation, the linearized momentum equation in terms of the x, y, and z components becomes

$$-i\omega v_{1xj} = \frac{q_j}{m_j}E_{1x} + \frac{q_j}{m_j}v_{1yj}B_0 - \frac{ikp_1}{m_j n_{0j}}, \tag{B7}$$

$$-i\omega v_{1yj} = \frac{q_j}{m_j}E_{1y} - \frac{q_j}{m_j}v_{1xj}B_0, \tag{B8}$$

$$-i\omega v_{1zj} = \frac{q_j}{m_j}E_{1z}, \tag{B9}$$

where we assumed that the background electric field is zero, $\mathbf{E}_0 = 0$. Our approach is to find a relationship between the velocities and the electric field in the form of $\widetilde{\mathbf{L}}_j\mathbf{v}_{1j} = \mathbf{E}_1$, where $\widetilde{\mathbf{L}}_j(\mathbf{k}, \omega)$ is a complex tensor. Solving for the velocities of each particle species, we can obtain the current density as $\mathbf{J}_1 = \sum_j n_{0j}q_j\mathbf{v}_{1j}$, which yields the relationship $\mathbf{J}_1 = \widetilde{\sigma}\mathbf{E}_1$, where $\widetilde{\sigma}$ is the conductivity tensor. From the conductivity tensor $\widetilde{\sigma}$, we obtain the susceptibility tensor $\widetilde{\chi}$, and finally the dielectric tensor $\widetilde{\mathbf{M}}$, using the standard definitions. Then we insert $\widetilde{\mathbf{M}}$ into equation (B3) to obtain the three-fluid dispersion relation for perpendicular waves.

Assuming adiabatic pressure perturbations for low-frequency waves, we can relate the change of pressure to the change of density through the following equation:

$$\frac{\partial p_j}{\partial t} = m_j c_j^2 \frac{\partial n_j}{\partial t}, \tag{B10}$$

where $c_j = \sqrt{\frac{\gamma_j p_{0j}}{m_j n_{0j}}}$ is the sound speed in fluid j, and γ_j is the adiabatic index of fluid j. The linearized form of equation (B10) is

$$-i\omega p_{1j} = -i\omega n_{1j} m_j c_j^2. \tag{B11}$$

Combining equations (B6) and (B11), we obtain the pressure perturbation in terms of the velocity

$$p_{1j} = \frac{m_j n_{0j} k c_j^2}{\omega} v_{1xj}. \tag{B12}$$

Substituting equation (B12) into equation (B7), we find the relation between the velocities and the electric field $\widetilde{\mathbf{L}}_j\mathbf{v}_{1j} = \mathbf{E}_1$ from equations (B7) to (B9) with

$$\widetilde{\mathbf{L}}_j = \begin{bmatrix} \left(\frac{-i\omega m_j}{q_j} + im_j k^2 c_j^2\right) & \frac{-\Omega_j m_j}{q_j} & 0 \\ \frac{\Omega_j m_j}{q_j} & \frac{-i\omega m_j}{q_j} & 0 \\ 0 & 0 & \frac{-i\omega m_j}{q_j} \end{bmatrix}, \tag{B13}$$

where $\Omega_j = \frac{q_j B_0}{m_j}$ is the gyrofrequency of particle species j. Here we use Ω_e with negative sign, because of the negative charge of electrons. Now we calculate the current density perturbation as $\mathbf{J}_1 = \sum_j n_{0j}q_j\widetilde{\mathbf{L}}_j^{-1}\mathbf{E}_1 = \widetilde{\sigma}\,\mathbf{E}_1$, where the conductivity tensor is

$$\widetilde{\sigma} = \begin{bmatrix} -i\sum_j \frac{n_{0j}q_j^2\omega}{m_j\left(c_j^2k^2 + \Omega_j^2 - \omega^2\right)} & \sum_j \frac{n_{0j}q_j^2\Omega_j}{m_j\left(c_j^2k^2 + \Omega_j^2 - \omega^2\right)} & 0 \\ -\sum_j \frac{n_{0j}q_j^2\Omega_j}{m_j\left(c_j^2k^2 + \Omega_j^2 - \omega^2\right)} & i\sum_j \frac{n_{0j}q_j^2\left(c_j^2k^2 - \omega^2\right)}{m_j\omega\left(c_j^2k^2 + \Omega_j^2 - \omega^2\right)} & 0 \\ 0 & 0 & i\sum_j \frac{n_{0j}q_j^2}{m_j\omega} \end{bmatrix}. \tag{B14}$$

From the conductivity tensor, we obtain the susceptibility tensor through the relation $\widetilde{\chi} = \frac{i}{\varepsilon_0 \omega}\widetilde{\sigma}$,

$$\widetilde{\chi} = \begin{bmatrix} \sum_j \frac{\omega_{pj}^2}{c_j^2 k^2 + \Omega_j^2 - \omega^2} & i\sum_j \frac{\omega_{pj}^2 \Omega_j}{\omega\left(c_j^2 k^2 + \Omega_j^2 - \omega^2\right)} & 0 \\ -i\sum_j \frac{\omega_{pj}^2 \Omega_j}{\omega\left(c_j^2 k^2 + \Omega_j^2 - \omega^2\right)} & -\sum_j \frac{\omega_{pj}^2\left(c_j^2 k^2 - \omega^2\right)}{\omega^2\left(c_j^2 k^2 + \Omega_j^2 - \omega^2\right)} & 0 \\ 0 & 0 & -\sum_j \frac{\omega_{pj}^2}{\omega^2} \end{bmatrix}, \tag{B15}$$

where $\omega_{pj} = \sqrt{\frac{n_{0j} q_j^2}{\varepsilon_0 m_j}}$ is the plasma frequency of particle species j, and ε_0 is the permittivity of free space. Finally, we use the definition $\widetilde{\mathbf{M}} = \widetilde{\mathbf{I}} + \widetilde{\chi}$ to obtain the dielectric tensor of warm multifluid plasma

$$\widetilde{\mathbf{M}} = \begin{bmatrix} 1 + \sum_j \frac{\omega_{pj}^2}{c_j^2 k^2 + \Omega_j^2 - \omega^2} & i\sum_j \frac{\omega_{pj}^2 \Omega_j}{\omega\left(c_j^2 k^2 + \Omega_j^2 - \omega^2\right)} & 0 \\ -i\sum_j \frac{\omega_{pj}^2 \Omega_j}{\omega\left(c_j^2 k^2 + \Omega_j^2 - \omega^2\right)} & 1 - \sum_j \frac{\omega_{pj}^2\left(c_j^2 k^2 - \omega^2\right)}{\omega^2\left(c_j^2 k^2 + \Omega_j^2 - \omega^2\right)} & 0 \\ 0 & 0 & 1 - \sum_j \frac{\omega_{pj}^2}{\omega^2} \end{bmatrix}. \tag{B16}$$

Substituting the dielectric tensor to equation (B3), we arrive at the dispersion relation of warm multifluid plasma for perpendicular wave propagation:

$$\left[\left(1 + \sum_j \frac{\omega_{pj}^2}{c_j^2 k^2 + \Omega_j^2 - \omega^2}\right)\left(1 - \sum_j \frac{\omega_{pj}^2\left(c_j^2 k^2 - \omega^2\right)}{\omega^2\left(c_j^2 k^2 + \Omega_j^2 - \omega^2\right)} - \frac{c^2 k^2}{\omega^2}\right) + \left(\sum_j \frac{\omega_{pj}^2 \Omega_j}{\omega\left(c_j^2 k^2 + \Omega_j^2 - \omega^2\right)}\right)^2\right] \times \left(1 - \sum_j \frac{\omega_{pj}^2}{\omega^2} - \frac{c^2 k^2}{\omega^2}\right) = 0 \tag{B17}$$

We can show that at the low-frequency (and low-wave number) limit,

$$1 << \left|\sum_j \frac{\omega_{pj}^2}{c_j^2 k^2 + \Omega_j^2 - \omega^2}\right|, \tag{B18}$$

provided that

$$1 \ll \sum_j \frac{\omega_{pj}^2}{\Omega_j^2} = \sum_j \frac{n_j m_j}{\varepsilon_0 B_0^2} = \frac{1}{\varepsilon_0 \mu_0 V_A^2} = \frac{c^2}{V_A^2},\ i.e.\ V_A \ll c, \tag{B19}$$

where V_A is the Alfvén speed in the compound system and μ_0 is the permeability of free space. At the termination shock $V_A \approx 30$ km/s, which is much less then the speed of light. Thus from equation (B17), we obtain the following dispersion relation for perpendicular magnetosonic waves

$$\left(\sum_j \frac{\omega_{pj}^2 \Omega_j}{\omega^2 - c_j^2 k^2 - \Omega_j^2}\right)^2 - \left(c^2 k^2 + \sum_j \frac{\omega_{pj}^2\left(\omega^2 - c_j^2 k^2\right)}{\omega^2 - c_j^2 k^2 - \Omega_j^2}\right)\left(\sum_j \frac{\omega_{pj}^2}{\omega^2 - c_j^2 k^2 - \Omega_j^2}\right) = 0. \tag{B20}$$

In case of three fluids, i.e., pickup ions, thermal solar wind ions and electrons, equation (B20) yields a second-order polynomial equation for ω^2 as given in [*Toida and Aota*, 2013]:

$$A_2(k)\omega^4 - A_1(k)\omega^2 + A_0(k) = 0, \tag{B21}$$

where

$$A_2 = \sum_j \omega_{pj}^2 \left(c^2 k^2 + \sum_j \omega_{pj}^2 \right), \tag{B22}$$

$$A_1 = \left(\sum_j \omega_{pj}^2 \sum_j \Omega_j^{*2} - \sum_j \omega_{pj}^2 \Omega_j^{*2} \right) \left(c^2 k^2 + \sum_j \omega_{pj}^2 \right) - \left[\omega_{pPUI}^2 \omega_{pSW}^2 (\Omega_{PUI} - \Omega_{SW})^2 + \omega_{pSW}^2 \omega_{pe}^2 (\Omega_{SW} - \Omega_e)^2 + \omega_{pe}^2 \omega_{pPUI}^2 (\Omega_e - \Omega_{PUI})^2 \right], \tag{B23}$$

$$A_0 = \left(\omega_{pPUI}^2 \Omega_{SW}^{*2} \Omega_e^{*2} + \omega_{pSW}^2 \Omega_e^{*2} \Omega_{PUI}^{*2} + \omega_{pe}^2 \Omega_{PUI}^{*2} \Omega_{SW}^{*2} \right) \left(c^2 k^2 + \sum_j \omega_{pj}^2 \right) - \left[\omega_{pPUI}^2 \omega_{pSW}^2 \Omega_e^{*2} (\Omega_{PUI} - \Omega_{SW})^2 + \omega_{pSW}^2 \omega_{pe}^2 \Omega_{PUI}^{*2} (\Omega_{SW} - \Omega_e)^2 + \omega_{pe}^2 \omega_{pPUI}^2 \Omega_{SW}^{*2} (\Omega_e - \Omega_{PUI})^2 \right], \tag{B24}$$

and

$$\Omega_j^{*2} = \Omega_j^2 + k c_j^2. \tag{B25}$$

In the above equations, the electron gyrofrequency is $\Omega_e = \frac{q_e B_0}{m_e} = -\frac{eB_0}{m_e} = -|\Omega_e|$, where e is the elementary charge. Solving the dispersion relation (B21) for ω, we find the frequencies for the high-frequency fast mode or pickup ion fast mode (F_{PUI}) and the low-frequency fast mode or thermal solar wind ion fast mode (F_{SW}):

$$\omega_{PUI} = \sqrt{\frac{A_1 + \sqrt{A_1^2 - 4A_2A_0}}{2A_2}}, \tag{B26}$$

$$\omega_{SW} = \sqrt{\frac{A_1 - \sqrt{A_1^2 - 4A_2A_0}}{2A_2}}. \tag{B27}$$

These are the frequencies of the two linear plane waves in the three-fluid solar wind plasma comprising thermal ions, pickup ions, and electrons. The phase velocities of F_{PUI} and F_{SW} can be calculated as $\frac{\omega_{PUI}}{k}$ and $\frac{\omega_{SW}}{k}$, respectively, which are plotted in Figure 1a.

To get the phase velocity of the quasi-stationary wave solutions, i.e., solitons and oscillitons, we need to solve equation (B21) for k as a function of the phase velocity $V_{ph} = \frac{\omega}{k}$ [*Sauer et al.*, 2001, 2003; *Dubinin et al.*, 2006]. Substituting the phase velocity into equation (B21), we can rewrite the linear dispersion relation as

$$k^4 A_2(k) V_{ph}^4 - k^2 A_1(k) V_{ph}^2 + A_0(k) = 0 \tag{B28}$$

Inserting equations (B22)–(B25) into equation (B28) and collecting the powers of k, we get a sixth-order polynomial equation for k:

$$B_3(V_{ph}) k^6 + B_2(V_{ph}) k^4 + B_1(V_{ph}) k^2 + B_0 = 0. \tag{B29}$$

This is a cubic equation for $z = k^2$:

$$B_3(V_{ph}) z^3 + B_2(V_{ph}) z^2 + B_1(V_{ph}) z + B_0 = 0, \tag{B30}$$

which can be solved analytically, as follows. If the discriminant Δ is positive, the cubic equation (B30) has three distinct real roots, $z_1, z_2,$, and z_3, where

$$\Delta = 18 B_3 B_2 B_1 B_0 - 4 B_2^3 B_0 + B_2^2 B_1^2 - 4 B_3 B_1^3 - 27 B_3^2 B_0^2. \tag{B31}$$

If Δ is zero, multiple roots exist. The solutions of equation (B30) are

$$z_1 = -\frac{1}{3B_3} \left(B_2 + u_1 C + \frac{\Delta_0}{u_1 C} \right), \tag{B32}$$

$$z_2 = -\frac{1}{3B_3} \left(B_2 + u_2 C + \frac{\Delta_0}{u_2 C} \right), \tag{B33}$$

$$z_3 = -\frac{1}{3B_3} \left(B_2 + u_3 C + \frac{\Delta_0}{u_3 C} \right), \tag{B34}$$

where $u_1 = 1$, $u_2 = \frac{-1+i\sqrt{3}}{2}$, $u_3 = \frac{-1-i\sqrt{3}}{2}$,

$$C = \sqrt[3]{\frac{\Delta_1 + \sqrt{\Delta_1^2 - 4\Delta_0^3}}{2}}, \tag{B35}$$

$$\Delta_0 = B_2^2 - 3B_3B_1, \tag{B36}$$

and

$$\Delta_1 = 2B_2^3 - 9B_3B_2B_1 + 27B_3^2B_0. \tag{B37}$$

Finally we find the six solutions $k = k(V_{ph})$:

$$k_1 = \sqrt{z_1},\ \ k_2 = \sqrt{z_2},\ \ k_3 = \sqrt{z_3},\ \ k_4 = -\sqrt{z_1},\ \ k_5 = -\sqrt{z_2},\ \text{ and }\ k_6 = -\sqrt{z_3}. \tag{B38}$$

The real and imaginary parts of k_1, k_2, and k_3 are plotted in Figure 2 for the upstream conditions at the termination shock crossing TS3.

If the $k = k(V_{ph})$ solution of the linear dispersion relation $D(\omega, k) = 0$ is real, the wave mode is a linear wave. If the solution is imaginary, the wave mode is a soliton. If the solution is complex, the wave mode is an oscilliton. Two complex solutions are found at the phase velocities of U_{fm} and c_{PUI}, where $U_{fm} = \sqrt{c_s^2 + V_A^2}$ is the fast magnetosonic speed of the total fluid with c_s and V_A being the sound and Alfvén speeds in the total fluid and c_{PUI} is the sound speed in the pickup ion fluid. The linear wave analysis presented here gives only the quasi-linear solution of solitons and oscillitons. We obtain the fully nonlinear oscilliton solution by solving the three-fluid MHD equations (equations (1)–(5)) numerically in our shock tube simulation, which results in a nonlinear quasi-stationary shock wave that appears as a standing wave train downstream of the termination shock.

Appendix C: Calculation of the Partial Pressure of Energetic Electrons

We calculated the partial pressure of energetic electrons just upstream of the termination shock from the observed differential intensities of the LECP instrument in the energy range 0.022–1.5 MeV.

The pressure is defined as the rate of momentum transfer in a given direction through a unit area per unit time. Assuming isotropic pressure, the momentum is randomly distributed in three dimensions, so the pressure is given by

$$P = \frac{1}{3}\int_0^\infty n(E)p(E)v(E)\mathrm{d}E, \tag{C1}$$

where $n(E)\mathrm{d}E$ is the number of particles between E and $E + \mathrm{d}E$ in a unit volume of the plasma, p is the magnitude of the momentum, and v is the speed associated with the kinetic energy E of the particle. From equation (C1) we get the partial pressure of energetic electrons within $\mathrm{d}E$ at E:

$$\mathrm{d}P = \frac{1}{3}n(E)\gamma_L(E)m_0v^2(E)\mathrm{d}E, \tag{C2}$$

where m_0 is the rest mass of electron and the Lorentz factor γ_L is defined as

$$\gamma_L = \frac{1}{\sqrt{1 - \frac{v^2}{c^2}}}, \tag{C3}$$

where c is the speed of light.

The differential intensity j is defined as

$$j(E) = \frac{n(E)v(E)}{4\pi}. \tag{C4}$$

Combining (C2) and (C4), we express the partial pressure in terms of the differential intensity:

$$\mathrm{d}P = \frac{4\pi}{3}j(E)\gamma_L(E)m_0v(E)\mathrm{d}E. \tag{C5}$$

For a finite energy channel the partial pressure can be calculated as

$$P(E_m) = \frac{4\pi}{3} j(E_m)\gamma_L(E_m)m_0 v(E_m)(E_2 - E_1), \tag{C6}$$

where E_1 and E_2 are the lower and upper cutoff energies of the channel and E_m is the geometric mean energy $E_m = \sqrt{E_1 E_2}$. Finally, the sum of the partial pressures of all channels gives the pressure of the LECP energetic electrons.

The number of electrons between E and $E + \mathrm{d}E$ in a unit volume of the plasma can be obtained from equation (C4):

$$n(E)\mathrm{d}E = j(E)\frac{4\pi}{v(E)}\mathrm{d}E, \tag{C7}$$

which gives the number density in a finite energy channel:

$$n(E_m) = j(E_m)\frac{4\pi}{v(E_m)}(E_2 - E_1). \tag{C8}$$

Acknowledgments

B.Z. and M.O. acknowledge the support of NASA Grand Challenge NNX14AIB0G and NASA Award NNX13AE04G. G.T. acknowledges support from the National Science Foundation grant AGS-1322543 and NASA Grand Challenge NNX14AIB0G. The high-resolution Voyager 2 plasma data used in this study are publicly available at the Voyager Data Page of the Massachusetts Institute of Technology Space Plasma Group: http://web.mit.edu/space/www/voyager/voyager_data/voyager_data.html. The 48 s resolution magnetic field data are accessible at the National Space Science Data Center: ftp://nssdcftp.gsfc.nasa.gov/spacecraft_data/voyager/voyager2/magnetic_fields/. The authors thank the two reviewers for their constructive comments.

Yuming Wang thanks Hans J. Fahr and one anonymous reviewer for their assistance in evaluating this paper.

References

Abraham-Shrauner, B. (1972), Determination of magnetohydrodynamic shock normals, *J. Geophys. Res.*, *77*, 736–739, doi:10.1029/JA077i004p00736.

Alouani-Bibi, F., M. Opher, D. Alexashov, V. Izmodenov, and G. Toth (2011), Kinetic versus multi-fluid approach for interstellar neutrals in the heliosphere: Exploration of the interstellar magnetic field effects, *Astrophys. J.*, *734*, 45, doi:10.1088/0004-637X/734/1/45.

Ariad, D., and M. Gedalin (2013), The role pickup ions play in the termination shock, *J. Geophys. Res. Space Physics*, *118*, 2854–2862, doi:10.1002/jgra.50170.

Balogh, A., and R. A. Treumann (2013), *Physics of Collisionless Shocks: Space Plasma Shock Waves*, Springer Science & Business Media, New York doi:10.1007/978-1-4614-6099-2.

Baumjohann, W., and R. A. Treumann (1996), *Basic Space Plasma Physics*, Imperial College Press, London.

Biskamp, D. (1973), Collisionless shock waves in plasmas, *Nucl. Fusion*, *13*, 719–740, doi:10.1088/0029-5515/13/5/010.

Burlaga, L. F., and N. F. Ness (2009), Compressible "turbulence" observed in the heliosheath by Voyager 2, *Astrophys. J.*, *703*, 311–324, doi:10.1088/0004-637X/703/1/311.

Burlaga, L. F., N. F. Ness, M. H. Acuña, R. P. Lepping, J. E. P. Connerney, and J. D. Richardson (2008), Magnetic fields at the solar wind termination shock, *Nature*, *454*, 75–77, doi:10.1038/nature07029.

Chalov, S. V., and H. J. Fahr (2013), The role of solar wind electrons at the solar wind termination shock, *Mon. Not. R. Astron. Soc. Lett.*, *433*, L40–L43, doi:10.1093/mnrasl/slt052.

Chashei, I. V., and H. J. Fahr (2014), On solar-wind electron heating at large solar distances, *Solar Phys.*, *289*, 1359–1370, doi:10.1007/s11207-013-0403-8.

Colburn, D. S., and C. P. Sonett (1966), Discontinuities in the solar wind, *Space Sci. Rev.*, *5*, 439–506, doi:10.1007/BF00240575.

Cummings, A. C., and E. C. Stone (2001), Inferring energetic particle mean-free paths from observations of anomalous cosmic rays in the outer heliosphere at solar maximum, in *Proceedings of the 27th International Cosmic Ray Conference*, vol. 10, pp. 4243–4246, Copernicus Systems and Technology GmbH, Berlin, Germany.

Decker, R. B., S. M. Krimigis, E. C. Roelof, M. E. Hill, T. P. Armstrong, G. Gloeckler, D. C. Hamilton, and L. J. Lanzerotti (2008), Mediation of the solar wind termination shock by non-thermal ions, *Nature*, *454*, 67–70, doi:10.1038/nature07030.

Dubinin, E. M., K. Sauer, and J. F. McKenzie (2006), Nonlinear 1-D stationary flows in multi-ion plasmas—sonic and critical loci—solitary and "oscillatory" waves, *Ann. Geophys.*, *24*, 3041–3057, doi:10.5194/angeo-24-3041-2006.

Dubinin, E., K. Sauer, and J. F. McKenzie (2004), Nonlinear stationary waves and solitons in ion beam-plasma configuration, *J. Geophys. Res.*, *109*, A02208, doi:10.1029/2003JA010283.

Fahr, H. J., and D. Rucinski (1999), Neutral interstellar gas atoms reducing the solar wind Mach number and fractionally neutralizing the solar wind, *Astron. Astrophys.*, *350*, 1071–1078.

Fahr, H. J., and S. V. Chalov (2008), Supersonic solar wind ion flows downstream of the termination shock explained by a two-fluid shock model, *Astron. Astrophys.*, *490*, L35–L38, doi:10.1051/0004-6361:200810679.

Fahr, H. J., I. V. Chashei, and D. Verscharen (2014), Traveling solar-wind bulk-velocity fluctuations and their effects on electron heating in the heliosphere, *Astron. Astrophys.*, *571*, A78, doi:10.1051/0004-6361/201424421.

Fahr, H. J., J. D. Richardson, and D. Verscharen (2015), The electron distribution function downstream of the solar-wind termination shock: Where are the hot electrons?, *Astron. Astrophys.*, *579*, A18, doi:10.1051/0004-6361/201525710.

Fitzpatrick, R. (2014), *Plasma Physics: An Introduction*, CRC Press, Boca Raton, Fla.

Florinski, V., R. B. Decker, J. A. le Roux, and G. P. Zank (2009), An energetic-particle-mediated termination shock observed by Voyager 2, *Geophys. Res. Lett.*, *36*, L12101, doi:10.1029/2009GL038423.

Fujii, Z., and F. B. McDonald (2005), The spatial distribution of galactic and anomalous cosmic rays in the heliosphere at solar minimum, *Adv. Space Res.*, *35*, 611–616, doi:10.1016/j.asr.2005.01.023.

Giacalone, J., and R. Decker (2010), The origin of low-energy anomalous cosmic rays at the solar-wind termination shock, *Astrophys. J.*, *710*, 91–96, doi:10.1088/0004-637X/710/1/91.

Giacalone, J., J. F. Drake, and J. R. Jokipii (2012), The acceleration mechanism of anomalous cosmic rays, *Space Sci. Rev.*, *173*, 283–307, doi:10.1007/s11214-012-9915-z.

Glocer, A., G. Tóth, Y. Ma, T. I. Gombosi, J.-C. Zhang, and L. M. Kistler (2009), Multifluid Block-Adaptive-Tree Solar wind Roe-type Upwind Scheme: Magnetospheric composition and dynamics during geomagnetic storms—Initial results, *J. Geophys. Res.*, *114*, A12203, doi:10.1029/2009JA014418.

Harnett, E. M., and R. M. Winglee (2006), Three-dimensional multifluid simulations of ionospheric loss at Mars from nominal solar wind conditions to magnetic cloud events, *J. Geophys. Res.*, *111*, A09213, doi:10.1029/2006JA011724.
Hoefer, M. A. (2014), Shock waves in dispersive Eulerian fluids, *J. Nonlinear Sci.*, *24*, 525–577, doi:10.1007/s00332-014-9199-4.
Isenberg, P. A. (1986), Interaction of the solar wind with interstellar neutral hydrogen—Three-fluid model, *J. Geophys. Res.*, *91*, 9965–9972, doi:10.1029/JA091iA09p09965.
Izmodenov, V. V., Y. G. Malama, M. S. Ruderman, S. V. Chalov, D. B. Alexashov, O. A. Katushkina, and E. A. Provornikova (2009), Kinetic-gasdynamic modeling of the heliospheric interface, *Space Sci. Rev.*, *146*, 329–351, doi:10.1007/s11214-009-9528-3.
Jokipii, J. R. (1966), Cosmic-ray propagation. I. Charged particles in a random magnetic field, *Astrophys. J.*, *146*, 480–487, doi:10.1086/148912.
Li, H., C. Wang, and J. D. Richardson (2008), Properties of the termination shock observed by Voyager 2, *Geophys. Res. Lett.*, *35*, L19107, doi:10.1029/2008GL034869.
Lu, Q., L. Shan, T. Zhang, G. P. Zank, Z. Yang, M. Wu, A. Du, and S. Wang (2013), The role of pickup ions on the structure of the Venusian bow shock and its implications for the termination shock, *Astrophys. J. Lett.*, *773*, L24, doi:10.1088/2041-8205/773/2/L24.
Najib, D., A. F. Nagy, G. Tóth, and Y. Ma (2011), Three-dimensional, multifluid, high spatial resolution MHD model studies of the solar wind interaction with Mars, *J. Geophys. Res.*, *116*, A05204, doi:10.1029/2010JA016272.
Opher, M., E. C. Stone, and P. C. Liewer (2006), The effects of a local interstellar magnetic field on Voyager 1 and 2 observations, *Astrophys. J. Lett.*, *640*, L71–L74, doi:10.1086/503251.
Opher, M., F. A. Bibi, G. Tóth, J. D. Richardson, V. V. Izmodenov, and T. I. Gombosi (2009), A strong, highly-tilted interstellar magnetic field near the Solar System, *Nature*, *462*, 1036–1038, doi:10.1038/nature08567.
Parker, E. N. (1958), Dynamics of the interplanetary gas and magnetic fields, *Astrophys. J.*, *128*, 664–676, doi:10.1086/146579.
Pogorelov, N. V., E. C. Stone, V. Florinski, and G. P. Zank (2007), Termination shock asymmetries as seen by the Voyager spacecraft: The role of the interstellar magnetic field and neutral hydrogen, *Astrophys. J.*, *668*, 611–624, doi:10.1086/520952.
Randol, B. M., D. J. McComas, and N. A. Schwadron (2013), Interstellar pick-up ions observed between 11 and 22 AU by New Horizons, *Astrophys. J.*, *768*, 120, doi:10.1088/0004-637X/768/2/120.
Ratkiewicz, R., and J. Grygorczuk (2008), Orientation of the local interstellar magnetic field inferred from Voyagers' positions, *Geophys. Res. Lett.*, *35*, L23105, doi:10.1029/2008GL036117.
Richardson, J. D., J. C. Kasper, C. Wang, J. W. Belcher, and A. J. Lazarus (2008), Cool heliosheath plasma and deceleration of the upstream solar wind at the termination shock, *Nature*, *454*, 63–66, doi:10.1038/nature07024.
Sauer, K., and E. Dubinin (2003), Oscillitons and gyrating ions in a beam-plasma system, *Geophys. Res. Lett.*, *30*(23), 2192, doi:10.1029/2003GL018266.
Sauer, K., E. Dubinin, K. Baumgärtel, and A. Bogdanov (1996), Bow shock splitting in bi-ion flows, *Geophys. Res. Lett.*, *23*, 3643–3646, doi:10.1029/96GL03425.
Sauer, K., E. Dubinin, and J. F. McKenzie (2001), New type of soliton in bi-ion plasmas and possible implications, *Geophys. Res. Lett.*, *28*, 3589–3592, doi:10.1029/2001GL013047.
Sauer, K., E. Dubinin, and J. F. McKenzie (2003), Solitons and oscillitons in multi-ion space plasmas, *Nonlinear Proc. Geophys.*, *10*, 121–130.
Soker, N., R. Rahin, E. Behar, and J. H. Kastner (2010), Comparing shocks in planetary nebulae with the solar wind termination shock, *Astrophys. J.*, *725*, 1910–1917, doi:10.1088/0004-637X/725/2/1910.
Stone, E. C., A. C. Cummings, F. B. McDonald, B. C. Heikkila, N. Lal, and W. R. Webber (2005), Voyager 1 explores the termination shock region and the heliosheath beyond, *Science*, *309*, 2017–2020, doi:10.1126/science.1117684.
Stone, E. C., A. C. Cummings, F. B. McDonald, B. C. Heikkila, N. Lal, and W. R. Webber (2008), An asymmetric solar wind termination shock, *Nature*, *454*, 71–74, doi:10.1038/nature07022.
Toida, M., and Y. Aota (2013), Finite beta effects on low- and high-frequency magnetosonic waves in a two-ion-species plasma, *Phys. Plasmas*, *20*(8), 082301, doi:10.1063/1.4817169.
Tóth, G., et al. (2012), Adaptive numerical algorithms in space weather modeling, *J. Comput. Phys.*, *231*, 870–903, doi:10.1016/j.jcp.2011.02.006.
Usmanov, A. V., and M. L. Goldstein (2006), A three-dimensional MHD solar wind model with pickup protons, *J. Geophys. Res.*, *111*, A07101, doi:10.1029/2005JA011533.
Usmanov, A. V., M. L. Goldstein, and W. H. Matthaeus (2014), Three-fluid, three-dimensional magnetohydrodynamic solar wind model with eddy viscosity and turbulent resistivity, *Astrophys. J.*, *788*, 43, doi:10.1088/0004-637X/788/1/43.
Vasyliunas, V. M., and G. L. Siscoe (1976), On the flux and the energy spectrum of interstellar ions in the solar system, *J. Geophys. Res.*, *81*, 1247–1252, doi:10.1029/JA081i007p01247.
Whang, Y. C. (1998), Solar wind in the distant heliosphere, *J. Geophys. Res.*, *103*(17), 17,419–17,428, doi:10.1029/98JA01524.
Wu, P., K. Liu, D. Winske, S. P. Gary, N. A. Schwadron, and H. O. Funsten (2010), Hybrid simulations of the termination shock: Suprathermal ion velocity distributions in the heliosheath, *J. Geophys. Res.*, *115*, A11105, doi:10.1029/2010JA015384.
Zank, G. P., H. L. Pauls, I. H. Cairns, and G. M. Webb (1996), Interstellar pickup ions and quasi-perpendicular shocks: Implications for the termination shock and interplanetary shocks, *J. Geophys. Res.*, *101*, 457–478, doi:10.1029/95JA02860.
Zank, G. P., W. H. Matthaeus, J. W. Bieber, and H. Moraal (1998), The radial and latitudinal dependence of the cosmic ray diffusion tensor in the heliosphere, *J. Geophys. Res.*, *103*, 2085–2097, doi:10.1029/97JA03013.
Zank, G. P., J. Heerikhuisen, N. V. Pogorelov, R. Burrows, and D. McComas (2010), Microstructure of the heliospheric termination shock: Implications for energetic neutral atom observations, *Astrophys. J.*, *708*, 1092–1106, doi:10.1088/0004-637X/708/2/1092.